JOURNAL OF GEOPHYSICAL RESEARCH, VOL. 112, D24205, doi:10.1029/2007JD008922, 2007

Examining feedbacks of aerosols to urban climate with a model that treats 3-D clouds with aerosol inclusions

Mark Z. Jacobson,[1] Yoram J. Kaufman,[2,4] and Yinon Rudich[3]

Received 7 May 2007; revised 26 June 2007; accepted 27 August 2007; published 28 December 2007.

[1] Anthropogenic aerosol particles alter clouds, radiation, and precipitation, thereby affecting weather, climate, and air pollution. To examine and understand such feedbacks, a module that simulates the evolution, movement, and microphysics of three-dimensional size-resolved mixed-phase clouds and precipitation and their multicomponent aerosol inclusions was developed and implemented into the GATOR-GCMOM global-through-urban air pollution-weather-climate model. A unique feature of the module is that aerosol particles and their chemical components are tracked in time and space within size-resolved liquid, ice, and graupel and interstitially within clouds. Modeled parameters were evaluated against in situ data, compared with MODIS climatologies, and nested with emission data down to 5 km resolution to study aerosol-cloud feedbacks in Los Angeles. Although updrafts are not resolved during deep convection at this resolution, most convection is shallow in Los Angeles. This resolution is also near the lower limit for which a hydrostatic solution to vertical momentum (used here) is similar to a nonhydrostatic solution. Aerosols in Los Angeles were found to increase cloud optical depth, cloud liquid water, cloud fraction, net downward thermal-infrared radiation, soil moisture, the relative humidity, and (slightly) middle-boundary layer air temperatures. Aerosols also decreased precipitation, surface solar, and near-surface temperatures. Both boundary layer warming due to black carbon and surface cooling due to all aerosol components increased stability, inhibiting cloud top growth under some conditions. Aerosols may feed back to themselves by increasing cloud liquid, gas dissolution, and aerosol volume upon evaporation. They may also decrease visibility by increasing the relative humidity and decrease photolysis below them by enhancing cloud thickness.

Citation: Jacobson, M. Z., Y. J. Kaufman, and Y. Rudich (2007), Examining feedbacks of aerosols to urban climate with a model that treats 3-D clouds with aerosol inclusions, *J. Geophys. Res.*, *112*, D24205, doi:10.1029/2007JD008922.

1. Introduction

[2] Aerosol particles (AP) affect the atmosphere in many ways. They change stability, vertical mixing, and the mixing depth [e.g., *Bergstrom and Viskanta*, 1973a, 1973b; *Venkatram and Viskanta*, 1977; *Ackerman*, 1977; *Jacobson*, 1997b, 1998; 2002b]. They increase cloud reflectivity [*Gunn and Phillips*, 1957; *Twomey*, 1977], suppress precipitation [*Gunn and Phillips*, 1957; *Warner*, 1968], and increase fractional cloudiness [*Albrecht*, 1989; *Rosenfeld*, 2000; *Borys et al.*, 2003; *Koren et al.*, 2005; *Kaufman et al.*, 2005]. By reducing precipitation, AP reduce wet removal of aerosol particles and gases, increasing their concentrations [*Jacobson*, 2002b; *Andreae et al.*, 2004] and reduce wind speeds and wind-driven emissions below them [Jacobson, 2002; *Jacobson and Kaufman*, 2006]. Absorbing AP decrease the relative humidity, affecting fractional cloudiness and stability [e.g., *Bretherton et al.*, 1995; *Klein*, 1997; *Hansen et al.*, 1997; *Ackerman et al.*, 2000; *Koren et al.*, 2004; *Feingold et al.*, 2005]. AP also increase the surface area and liquid volume available for trace-gas condensation and dissolution, respectively [*Jacobson*, 2002b]. Finally, AP change photolysis coefficients by scattering or absorbing UV radiation directly [*Jacobson*, 1997b, 1998; *Dickerson et al.*, 1997].

[3] To improve estimates of aerosol feedbacks to clouds and urban, regional, and global climate, it is important to treat the evolution of discretized size- and composition-resolved aerosols into discretized size-resolved clouds and precipitation. For example, *Zhang et al.* [2002] found that, under the assumption of uniform aerosol composition versus size, modal treatment of prognostic aerosol particle number and mass resulted in similar total particle number to but different size distributions from discretized (size-resolved) treatments

[1]Department of Civil and Environmental Engineering, Stanford University, Stanford, California, USA.
[2]NASA Goddard Space Flight Center, Greenbelt, Maryland, USA.
[3]Department of Environmental Sciences, Weizmann Institute of Science, Rehovot, Israel.
[4]Deceased 31 May 2006.

0148-0227/07/2007JD008922$09.00

following aerosol activation. Modal distributions also "fail(ed) to predict the size transition for activated particles." That study assumed similar composition as a function of size in both distributions. *Jacobson* [2003, Figure 5] showed that treating multiple aerosol discretized distributions, each of different composition as a function of size, resulted in significantly different cloud drop size distributions than treating the same multiple aerosol distributions with uniform composition due to the fact that different distributions with different compositions activate at different diameters. Treating multicomponent distributions could explain the dual peaks in cloud size distributions that are observed at times.

[4] Since it is not possible to treat the variation of particle composition with size in a mode, the representation of a particle size distribution with 1–3 modes rather than a discrete size distribution induces error. For example, emitted fossil-fuel soot composition varies with size, even between 1–100 nm [e.g., *Kittelson*, 1998], and physical/chemical processes affect aerosol composition differently with each small size increment [e.g., *Jacobson*, 2002a, Figures 3–8]. A modal representation with 1–3 modes does not account for these variations. Partly for these reasons, *Zhang et al.* [1999] concluded, "...with appropriate numerical algorithms and size resolution, a sectional representation can predict more accurate chemical composition and size distribution than a modal representation," although they found that, in the absence of precipitation, the modal representation predicted total aerosol mass and number reasonably. In the presence of precipitation, though, the use of modal clouds and aerosols prevents physical treatment of aerosol washout, since washout occurs upon interactions of each aerosol size with each precipitation size, but modal clouds/aerosols do not have sizes, so modal washout must be treated empirically. Similarly, treatment of rainout requires size resolution to account for different fall speeds of different sizes, so modal rainout must be parameterized.

[5] Due to the speed of the modal representation, nearly all global-scale aerosol-cloud interaction models to date have treated aerosols as modal or bulk parameters [e.g., *Lohmann et al.*, 2000; *Ghan et al.*, 2001; *Easter et al.*, 2004; *Takemura et al.*, 2005; *Storelvmo et al.*, 2006]. One global model has treated the evolution of size- and composition-resolved clouds from size- and composition-resolved aerosol particles [*Jacobson*, 2002b, 2003].

[6] On cloud scales, several 0-, 1-, and 2-D models have treated the evolution of size-resolved clouds from either modal or size-resolved aerosol particles [e.g., *Danielsen et al.*, 1972; *Hall*, 1980; *Tzivion et al.*, 1994; *Ackerman et al.*, 1995; *Reisin et al.*, 1996; *Feingold et al.*, 1996; *Zhang et al.*, 2002; *Abdul-Razzak and Ghan*, 2004; *Fantoukis and Nenes*, 2005] or empirically determined aerosol number concentration [e.g., *Segal et al.*, 2004; *Khain et al.*, 2004]. Several 3-D models have treated the evolution of bulk (non-size-resolved) cloud liquid and ice [e.g., *Klemp and Wilhelmson*, 1978; *Clark*, 1979; *Proctor*, 1989; *Wang and Chang*, 1993; *Skamarock et al.*, 1994; 2005; *Lee and Park*, 1994; *Chen and Lamb*, 1999; *Walko et al.*, 1995; *Molders and Olson*, 2004].

[7] Fewer 3-D models have treated size-resolved clouds and precipitation. *Lynn et al.* [2005] treated size-resolved liquid and ice evolving from empirically determined activated cloud condensation nuclei and ice deposition nuclei consisting of an assumed chemical. *Kogan* [1991], *Feingold and Kreidenweis* [2002], *Jiang et al.* [2002], and *Ackerman et al.* [2003] treated the evolution of size-resolved liquid clouds from discrete size resolved aerosol particles; *Ovtchinnikov and Kogan* [2000] did the same for mixed phase clouds.

[8] To date, no aerosol-cloud interaction model has tracked the time- and 3-D spatial evolution through mixed-phase clouds of discrete size-resolved aerosol particles containing multiple chemical components nor treated the physical interactions of discrete size- and composition-resolved interstitial aerosol particles with size- and composition-resolved clouds and the resulting radiative effects. Previously, *Jacobson* [2002b, 2003] developed a model that treated discrete size- and composition-resolved aerosol and liquid/ice/graupel hydrometeor particles for 3-D application on all scales, but clouds formed only vertically and were not transported horizontally. *Feingold and Kreidenweis* [2002] treated transfer of ammonium sulfate aerosol to liquid cloud drops, but stored the ammonium sulfate in two size bins independent of the liquid bins. The two bins were transported in 3-D but were unaffected by aerosol-hydrometeor or hydrometeor-hydrometeor coagulation or cold-cloud processes. *Ackerman et al.* [2003] treated transfer of one aerosol component to liquid cloud drops and tracked the core in each liquid bin during 3-D transport and hydrometeor-hydrometeor coagulation, but did not treat aerosol-hydrometeor coagulation or cold cloud processes. *Easter et al.* [2004] tracked aerosols scavenged by clouds in each column of a global model over a specific time interval, but aerosols were modal and not stored as a function of cloud drop size since the cloud distribution was also modal, and each aerosol mode did not contain multiple chemicals that varied with size. Here, an existing nested global-through-urban-scale model is modified to treat the horizontal and vertical 3-D, time-dependent evolution of size- and composition-resolved mixed-phase clouds and precipitation from size- and composition-resolved aerosol particles.

[9] The model is applied with high-resolution emissions to study the feedbacks of anthropogenic aerosol particles and their precursor gases (AAPPG) on clouds, precipitation, radiation, temperatures, and other parameters in the heavily polluted South Coast Air Basin (SCAB), California, USA, at a resolution near 5 km. AAPPG represent the difference between current and preindustrial human contribution to atmospheric gas and aerosol pollution. Trace gases in AAPPG (section 4) enhance not only aerosol formation but also gas-phase photochemical smog formation. The main purpose of this paper is to develop a better understanding of the effects of ambient aerosol particles resulting from AAPPG emissions on atmospheric properties with a physically based, high-resolution model that uses realistic gas and particle emission inventories. Below, the model, modifications to it, and its application to the SCAB are described.

2. Description of the Model

[10] The model modified here was GATOR-GCMOM, a one-way-nested global-through-urban Gas, Aerosol, Trans-

port, Radiation, General Circulation, Mesoscale, and Ocean Model [*Jacobson*, 1997a, 1997b, 2001a, 2001b, 2004, 2006]. Three nested domains were used: global (4°-SN × 5°-WE resolution), California (0.2° × 0.15° ≈ 21.5 km × 14.0 km) and South Coast Air Basin (SCAB) (0.045° × 0.05° ≈ 4.7 km × 5 km). The global domain included 39 sigma-pressure layers to 0.425 hPa. Regional domains included 26 layers to 103.5 hPa, each matching the bottom 26 global layers. All domains included five layers in the bottom 1 km. All processes were treated the same in all nested domains, except that dynamical and cloud treatments differed between global and regional domains.

[11] In the global domain, dynamics was solved with the hydrostatic potential-enstrophy, mass, and energy-conserving scheme of *Arakawa and Lamb* [1981]. In regional domains, the hydrostatic solution conserved enstrophy, mass, and kinetic energy [*Lu and Turco*, 1995]. Gas, aerosol, and hydrometeor (added here) transport was solved with the scheme of *Walcek and Aleksic* [1998] using modeled online winds and vertical diffusion coefficients.

[12] Section 3 discusses the new urban/regional 3-D cloud module in which size- and composition-resolved cloud and precipitation liquid, ice, and graupel form at the grid scale and are transported over time in 3-D. Cloud-aerosol microphysics is also size-resolved and time-dependent. For the global domain, clouds were treated as forming in subgrid columns with unique bases and tops. Thermodynamics and microphysics were solved as in *Jacobson* [2003, 2006]. Clouds were not transported horizontally, but column cloud-aerosol microphysics was solved explicitly and size-resolved cloud particles interacted and developed from size-resolved aerosol particles.

[13] Aerosol processes were treated in all domains as in *Jacobson* [2002a, 2005a]. The aerosol size distribution consisted of 17 size bins from 0.002 to 50 μm in diameter and 17 chemicals per bin. Particle number and component mole concentrations were tracked in time over the moving-center size structure. Single-particle volume was calculated assuming particles contained solution and nonsolution components. Sulfuric acid binary (at low ammonia) and ternary homogeneous nucleation [*Napari et al.*, 2002] and condensation were solved together between a gas and all aerosol size bins with a scheme that also solved organic gas condensation. The model also solved nonequilibrium dissolutional growth of inorganics (e.g., NH_3, HNO_3, HCl) and soluble organics to all sizes, internal aerosol equilibrium chemistry, and size-resolved aerosol-aerosol coagulation. Gas photochemistry among 126 gases and 283 reactions was calculated with the sparse-matrix solver, SMVGEAR II.

[14] Radiative transfer through gases, aerosol particles, and hydrometeor particles for heating rates and photolysis was solved [*Toon et al.*, 1989] for >600 spectral intervals. Infrared gas absorption was calculated as in the study of *Jacobson* [2005b]. Aerosol optical calculations assumed that black carbon (BC) (if present) comprised a particle's core and all other solution and nonsolution components coated the core. Cloud optical calculations assumed BC was surrounded by a spherical liquid water or nonspherical ice crystal shell. The surface albedos of snow, sea ice, and water (ocean and lake) were wavelength-dependent and predicted.

[15] The model treated ground temperature and moisture over subgrid soil, road, rooftop, and water surfaces, vegetation over soil, snow over bare soil, snow over vegetation over soil, sea-ice over water, and snow over sea-ice over water. Ocean mixed-layer depths, velocities, temperatures, energy transport, and mass transport were calculated with a gridded 2-D potential enstrophy-, kinetic energy-, and mass-conserving shallow-water equation module forced by wind stress in which sea-surface temperatures were predicted [*Ketefian*, 2006]. Nine layers existed below each ocean mixed-layer grid cell to treat energy and chemical diffusion to the deep ocean and ocean chemistry [*Jacobson*, 2005c].

3. Modifications for 3-D Cloud Evolution

[16] Cumulus parameterizations assume that the area of a grid cell is much greater (e.g., >20 km) than that occupied by an ensemble of subgrid clouds. Because individual clouds vary from tens to a few thousand meters, neither a cumulus parameterization nor explicit cloud treatment applies strictly at 5–20 km resolution although both methods produce stable results at this resolution. Here, an algorithm was developed to treat the explicit 3-D evolution and movement of size- and composition-resolved clouds and precipitation with aerosol inclusions and applied at ~5 km resolution. Characteristics of the algorithm are described in Table 1 and compared with two mesoscale models and a large-eddy simulation model. Of significant difference is that the mesoscale models, which are often run at the same horizontal resolution as the study here, do not transport clouds in 3-D or include discrete size- and composition-resolved cloud microphysics as treated here.

[17] Water vapor and aerosol particles are transported in the model by horizontal and vertical winds. When the air becomes supersaturated, condensation or deposition occurs. If clouds pre-exist, hydrometeor particles compete with interstitial aerosol particles for available water vapor. The ordinary differential equations solved here for water vapor condensation (evaporation) onto (from) aerosol particles (equation 1), deposition (sublimation) onto (from) aerosol particles (equation 2), condensation (evaporation) or deposition (sublimation) onto (from) pre-existing hydrometeor particles (liquid, ice, and/or graupel) (equation 3), and mole conservation (equation 4) are

$$\frac{dc_{L,Ni,t}}{dt} = k_{L,Ni,t-h}\left(C_{v,t} - S'_{L,Ni,t-h}C_{s,L,t-h}\right) \quad (1)$$

$$\frac{dc_{I,Ni,t}}{dt} = k_{I,Ni,t-h}\left(C_{v,t} - S'_{I,Ni,t-h}C_{s,I,t-h}\right) \quad (2)$$

$$\frac{dc_{H,Mj,t}}{dt} = k_{H,Mj,t-h}\left(C_{v,t} - S'_{H,Mj,t-h}C_{s,H,t-h}\right) \quad (3)$$

Table 1. Characteristics of the New 3-D Cloud Scheme in GATOR-GCMOM and a Comparison With the Cloud Treatments in Two Other Models That Treat Aerosols and Clouds and Their Feedback to Meteorology on the Mesoscale, the Weather Research and Forecasting Modeling System [*Skamarock et al.*, 2005; *Fast et al.*, 2006] and MM5-SBM [*Lynn et al.*, 2005], and One Large-Eddy Simulation Model [*Ackerman et al.*, 2003] (LES A03)[a]

	GATOR-GCMOM	WRF-CHEM	MM5-SBM	LES A03
What is the largest scale of nested domains?	Global	Regional	Regional	None
Is finest domain convection from cumulus param. or model dynamics?	MD	CP	CP	MD
Is the vertical motion equation nonhydrostatic (N) or hydrostatic (H)?	H	N	N	N
Can updrafts within clouds be tilted?	Yes	No	No	Yes
Are hydrometeor distributions discretely size resolved or bulk?	SR	Bulk	SR	SR
Are cloud liquid, ice, and graupel treated?	Yes (SR)	Yes (bulk)	Yes (SR)	Liq. (SR)
Are rain, snow, and hail treated?	Yes (SR)	Yes (bulk)	Yes (SR)	Rain (SR)
Do hydrometeor particles contain multiple-component inclusions?	Yes	No	No	1 compon.
Do hydrometeor particles move in 3-D over time?	Yes (SR)	No	No	Yes (SR)
Do inclusions within hydrometeor particles move in 3-D over time?	Yes (SR)	No	No	Yes (SR)
Are aerosols distributions discretely size-resolved or bulk?	SR	SR	Bulk	SR
Are multiple or single aerosol distributions treated?	Multiple	Single	Single	Single
Do aerosol particles of each size contain multiple components?	Yes	Yes	No	No
Do multiple aerosol size distributions coagulate among each other?	Yes	No	No	No
Do components within each aerosol distribution c oagulate with other distributions	Yes	No	No	No
Are CCN/IDN number empirical functions of supersaturation?	No	Yes (bulk)	Yes (bulk)	No
Are CCN/IDN number from the Kohler equation applied to the aerosol distributions?	Yes (SR)	No	No	Yes (SR)
Does water vapor grow onto size-/composition-resolved CCN/IDN?	Yes (SR)	No	No	Yes (SR)
Does water vapor grow onto an assumed CCN/IDN size distribution	No	No	Yes (SR)	No
Is water vapor growth solved competitively onto CCN and IDN, conserving water mass, when mixed-phase clouds exist?	Yes	No	No	No
Do hydrometeor particles of each size contain all aerosol chemical components they form on?	Yes	No	No	Yes
Are gases, aerosol components, and hydrometeor components transported with the same transport scheme?	Yes	No	No	1 compon. Yes
Are cloud particles converted to precipitation by autoconversion?	No	Yes	No	No
Do hydrometeor particles undergo SR liquid-liquid, liquid-ice, liquid-graupel, ice-ice, ice-graupel, graupel-graupel coagulation to form larger hydrometeor particles, including precipitation?	Yes (SR)	No	Yes (SR)	Yes (SR)
Do interstitial SR aerosols coagulate with SR liquid, ice, and graupel hydrometeor particles and their aerosol inclusions?	Yes (SR)	No	No	Liq-liq. No
Are aerosol inclusions tracked during hydromet.-hydromet. coag.?	Yes (SR)	No	No	Yes (SR) 1 compon.
Are aerosol inclusions tracked during aerosol-hydromet. coagulation?	Yes (SR)	No	No	No
Do large liquid drops break up?	Yes (SR)	No	Yes (SR)	No
Does drop breakup move aerosol inclusions with drop fragments?	Yes (SR)	No	No	No
Is heterogeneous-homogeneous freezing treated?	Yes (SR)	Yes (bulk)	Yes (SR)	No
Is contact freezing of aerosol particles with liquid drops treated?	Yes (SR)	No	No	No
Is evaporative freezing (due to evaporative cooling) treated?	Yes (SR)	No	No	No
Are ice and graupel melting treated?	Yes (SR)	Yes (bulk)	Yes (bulk)	No
Is hydrometeor settling treated?	Yes (SR)	Yes (bulk)	Yes (SR)	Yes (SR)
Are aerosol inclusions released upon evaporation, sublimation?	Yes (SR)	No	No	No
Do gases dissolve in and evaporate from hydrometeor particles?	Yes (SR)	No	No	No
Is aqueous chemistry within liquid drops treated?	Yes (SR)	No	No	No
Is lightning from charge separation during SR hydrometeor-hydrometeor coagulation bounceoff treated?	Yes (SR)	No	No	No
Is radiative transfer through interstitial aerosol particles treated?	Yes (SR)	No	No	Yes (SR)
Is radiative transfer through hydrometeor particles treated?	Yes (SR)	Yes (bulk)	Yes (bulk)	Yes (SR)

[a]SR = size-resolved. N/A = not applicable. CCN = cloud condensation nuclei. IDN = ice deposition nuclei.

$$\frac{dC_{v,t}}{dt} = -\sum_{N=1}^{N_T}\sum_{i=1}^{N_B}\left[k_{L,Ni,t-h}\left(C_{v,t} - S'_{L,Ni,t-h}C_{s,L,t-h}\right) + k_{I,Ni,t-h}\left(C_{v,t} - S'_{I,Ni,t-h}C_{s,I,t-h}\right)\right] - \sum_{M=1}^{N_H}\sum_{j=1}^{N_C}\left[k_{H,Mj,t-h}\left(C_{v,t} - S'_{H,Mj,t-h}C_{S,M,t-h}\right)\right] \quad (4)$$

respectively. In these equations, t and t-h are the end and beginning, respectively of a time step of h seconds, subscripts L, I, and H identify new liquid hydrometeor particles from aerosol particles, new ice hydrometeor particles from aerosol particles, and preexisting hydrometeor particles, respectively, subscripts N and i indicate the aerosol size distribution from which new hydrometeor particles originate and the size bin in the distribution, respectively, subscripts M and j indicate a preexisting hydrometeor size distribution and a size bin in the distribution, respectively, N_T and N_B are the number of aerosol size distributions (1 in the present study) and size bins per distribution (17 in the present study), respectively, N_H and N_C are the number of hydrometeor size distributions (3: liquid, ice, and graupel) and size bins per distribution (12, ranging from 0.5-μm to 8-mm diameter in the present study), respectively, $c_{L,Ni}$, $c_{I,Ni}$, $c_{H,Mj}$ are mole concentrations (moles per cubic centimeter of air) of liquid water going to an aerosol distribution, ice going to an aerosol distribution, and liquid water or ice going to a preexisting liquid, ice, or graupel hydrometeor distribution, respectively, C_v is the ambient water vapor mole concentration, C_s is the saturation vapor mole concentration over a flat, dilute liquid water or ice surface, S' is the saturation ratio at equilibrium of water vapor over a liquid solution or ice surface, and $k_{L,Ni}$, $k_{I,Ni}$, and $k_{H,Mj}$ are mass transfer rates (s^{-1}) of water vapor to a liquid aerosol surface, ice aerosol surface, or pre-existing hydrometeor (liquid, ice, or graupel) particle surface, respectively [*Jacobson*, 2003, equations 12–13].

[18] The saturation ratios at equilibrium (S') are determined from Köhler theory as a function of aerosol particle composition and size, accounting for the Kelvin effect and Raoult's law for liquid activation and the Kelvin effect for ice activation. Aerosol composition of a given size affects the Kelvin term through the surface tension and Raoult's law through the molality term [*Jacobson*, 2003, equations 7–8]. Treatment of surface tension due to organics and inorganics is described by *Jacobson* [2005d, equations 16.34 and 16.35, respectively]. Ice nuclei included fractional numbers of pollen, spores, bacteria, soil dust, sodium, chloride, and other aerosol chemicals [e.g., *Jacobson*, 2003].

[19] The saturation vapor mole concentration over a flat, dilute liquid water surface ($C_{s,L}$) is determined in each grid cell and time step by iterating bulk condensation and latent heat exchange equations starting with the initial water vapor mole concentration and temperature in the grid cell, until the ambient and saturation mole concentrations are equal and in equilibrium with the temperature. The saturation vapor mole concentration over ice ($C_{s,I}$) is iterated to determine the equilibrium temperature as well under subfreezing conditions. The actual temperature change in the grid cell due to condensation/deposition is determined following the solution to equations 1–4. This temperature change feeds back to the dynamics calculation, driving horizontal and vertical velocities and pressure, which affect moisture, gas, and aerosol transport for the next time step in the 3-D model.

[20] The solution to this new set of equations, which describes simultaneous growth onto aerosol and hydrometeor particles, is an extension of that by *Jacobson* [2003], which considered growth onto aerosol particles but not preexisting hydrometeor particles. Integrating equations 1–3 for one size bin over a time step h gives

$$c_{L,Ni,t} = c_{L,Ni,t-h} + hk_{L,Ni,t-h}\left(C_{v,t} - S'_{L,Ni,t-h}C_{s,L,t-h}\right) \quad (5)$$

$$c_{I,Ni,t} = c_{I,Ni,t-h} + hk_{I,Ni,t-h}\left(C_{v,t} - S'_{I,Ni,t-h}C_{s,I,t-h}\right) \quad (6)$$

$$c_{H,Mj,t} = c_{H,Mj,t-h} + hk_{H,Mj,t-h}\left(C_{v,t} - S'_{H,Mj,t-h}C_{s,M,t-h}\right) \quad (7)$$

respectively, where the final gas mole concentration, $C_{v,t}$, is currently unknown. The solution assumes that equations are solved over all preexisting hydrometeor size bins and over those aerosol size bins (in equations 5 and 6) in which aerosol particles can activate to cloud drops. The criteria for activation are given in *Jacobson* [2003]. Some preexisting hydrometeor particles grow; others shrink during the calculation. Final hydrometeor and gas concentrations are constrained by the gas-hydrometeor mass balance equation,

$$C_{v,t} + \sum_{N=1}^{N_T}\sum_{i=1}^{N_B}\left(c_{L,Ni,t} + c_{I,Ni,t}\right) + \sum_{M=1}^{N_H}\sum_{j=1}^{N_C}c_{H,Mj,t} = C_{v,t-h} + \sum_{N=1}^{N_T}\sum_{i=1}^{N_B}\left(c_{L,Ni,t-h} + c_{I,Ni,t-h}\right) + \sum_{M=1}^{N_H}\sum_{j=1}^{N_C}c_{H,Mj,t-h} = C_{tot} \quad (8)$$

Substituting equations 5–7 into equation 8 and solving for $C_{v,t}$ gives a generalized solution for simultaneous condensation/evaporation and deposition/sublimation,

$$C_{v,t} = \frac{C_{v,t-h} + h\sum_{N=1}^{N_T}\sum_{i=1}^{N_B}\left(k_{L,Ni,t-h}S_{L,Ni,t-h}C_{s,L,t-h} + k_{I,Ni,t-h}S_{I,Ni,t-h}C_{s,I,t-h}\right) + h\sum_{M=1}^{N_H}\sum_{j=1}^{N_C}k_{H,Mj,t-h}S_{H,Mj,t-h}C_{s,M,t-h}}{1 + h\sum_{N=1}^{N_T}\sum_{i=1}^{N_B}\left(k_{L,Ni,t-h} + k_{I,Ni,t-h}\right) + h\sum_{M=1}^{N_H}\sum_{j=1}^{N_C}k_{H,Mj,t-h}} \quad (9)$$

Equation 9 must be limited by $C_{v,t} = \mathrm{MIN}(C_{v,t}, C_{tot})$, since evaporation can result in a gas concentration above the maximum available. Equation 9 cannot fall below zero in any situation. Next, $C_{v,t}$ is substituted into equations 5–7 to give the final hydrometeor concentrations in each size bin. Since equations 5–7 can result in concentrations below zero or above the maximum, two limits are placed sequentially, after they have been solved. The first is $c_{L,N,i,t} = \mathrm{MAX}(c_{L,N,i,t},0)$; $c_{I,N,i,t} = \mathrm{MAX}(c_{I,N,i,t},0)$; $c_{H,Mj,t} = \mathrm{MAX}(c_{H,Mj,t},0)$. The second, shown for liquid growth onto CCN, is

$$c_{L,Ni,t} = \frac{C_{v,t-h} - C_{v,t} + \sum_{N=1}^{N_T}\sum_{i=1}^{N_B}\left\{\mathrm{MAX}\left[c_{L,Ni,t-h} - c_{L,Ni,t},0\right] + \mathrm{MAX}\left[c_{I,Ni,t-h} - c_{I,Ni,t},0\right]\right\} + \sum_{M=1}^{N_H}\sum_{j=1}^{N_C}\mathrm{MAX}\left[c_{H,Mj,t-h} - c_{H,Mj,t},0\right]}{\sum_{N=1}^{N_T}\sum_{i=1}^{N_B}\left\{\mathrm{MAX}\left[c_{L,Ni,t} - c_{L,Ni,t-h},0\right] + \mathrm{MAX}\left[c_{I,Ni,t} - c_{I,Ni,t-h},0\right]\right\} + \sum_{M=1}^{N_H}\sum_{j=1}^{N_C}\mathrm{MAX}\left[\mathrm{c_{H,Mj,t}} - \mathrm{c_{H,Mj,t-h}},0\right]} \cdot \left(c_{L,Ni,t} - c_{L,Ni,t-h}\right) \quad (10)$$

where $c_{L,N,i,t}$, $c_{I,N,i,t}$, and $c_{H,Mj,t}$ on the right side are determined from equations 5–7, respectively, after the first limit above has been applied. The equation for ice growth onto IDN uses $c_{I,Ni,t}-c_{I,Ni,t-h}$ instead of $c_{L,Ni,t}-c_{L,Ni,t\text{-}h}$ in the rightmost term in equation 10. The equation for growth onto preexisting hydrometeor particles is analogous. Equation 10 states that the final concentration equals the net vapor loss due to growth ($C_{v,t-h}-C_{v,t}$) plus the vapor gain due to evaporation/sublimation, all scaled by the ratio of condensation into the bin ($c_{L,N,i,t}-c_{L,N,i,t-h}$) to condensation and deposition into all bins. The solution in equations 5–10 is exactly mole conserving between the gas and hydrometeors under all conditions and is noniterative and positive-definite. *Jacobson* [2003] analyzes results with the scheme applied to growth onto aerosol particles only.

[21] Remaining microphysical treatments (e.g., coagulation freezing, melting, chemistry, etc.) are as in the work of *Jacobson* [2003], except that the lightning treatment is given by *Jacobson* [2005d, Section 18.8.11]. During all microphysical and transport calculations, energy, water, and all chemicals are conserved over the 3-D model. Latent heat released and absorbed during cloud formation and decay feed back to meteorology through the thermodynamic energy equation.

[22] One disadvantage of the current study is that vertical velocities are calculated under a hydrostatic rather than nonhydrostatic assumption. However, *Stadlbacher* [Nonhydrostatic vs. hydrostatic on high resolution, www.cnrm.meteo.fr/aladin/meetings/Toulouse2001/RAPPORTS/Rapport_KS.aw.ps.gz], *Niemela and Fortelius* [Representation of convection under hydrostatic and nonhydrostatic HIRLAM: a case study of the convective event. DWD Forschung und Entwicklung Arbeitsergebnisse, 78, 5th International SRNWP-Workshop on Non-hydrostatic Modeling in Bad Orb, Germany, 27–29 Oct., 2003), and *Janjic and DiMego* [Alternative non-hydrostatic meso model applied to the Wasatch Mountain Wind Storm of 2/24/97, www.emc.ncep.noaa.gov/mmb/papers/janjic/9911/zj9911.htm, 2004] found that, in cloud cases with parameterized convection, differences between the two were small at 5 km, 5.5 km and 8 km resolution, respectively. *Stadlbacher* further found that, while errors increased from 5 km to 2.5 km, "the differences between using nonhydrostatic or hydrostatic dynamics are small compared to other changes." Because the finest spacing used here is 4.7 km × 5 km, use of the hydrostatic assumption may have little effect on the conclusions of this study, according to these previous studies. Further, the use of a hydrostatic model here is not a necessary condition for running the model, as the hydrostatic dynamics will be replaced by a nonhydrostatic scheme that conserves potential enstrophy, total energy, mass, and potential enthalpy [*Ketefian*, 2006], but such a conversion will take time.

[23] Another shortcoming of the current study is the resolution. Ideally, clouds would be resolved at 1 km or less rather than 5 km, since updrafts during deep convection cannot be resolved at 5 km resolution, limiting the accuracy of modeled supersaturations. An alternative method of modeling supersaturations at coarse resolution is with a diagnostic scheme. For example, *Nenes and Seinfeld* [2003] used an adiabatic parcel model with a constant updraft velocity to determine the maximum supersaturation found during the ascent of a cloud parcel. Such a model can predict cloud activation well at cloud base. Diagnostic schemes can also predict activation in the interior of convective clouds if the supersaturation is calculated correctly [e.g., *Phillips et al.*, 2007]. However, diagnostic schemes may be limited when updrafts are not vertical, such as in severe thunderstorms and when significant entrainment occurs due to shear-driven turbulence (since the parcel movement is no longer adiabatic). The 3-D treatment of clouds, while not resolving updrafts well in the current study, does treat ascent in the presence of wind shear and strong entrainment. Thus as the resolution increases, it should approach a better solution.

[24] Further, the purpose of this study is to examine the effects of aerosols on clouds over a large region, approximately 350 km × 216 km. The computer time for one month of simulation over such a domain at 1 km × 1 km

resolution with the treatment of chemistry, aerosols, radiation, and clouds here would be about two years; thus at 1 km × 1 km resolution, the domain must be limited and clouds could not be resolved over much of it due to computational constraints. Thus although the coarser model resolution is less accurate in each location, particularly with respect to deep convection, it may be more accurate overall than not treating a large portion of the domain. All global and mesoscale model studies at 5 km resolution or lower to date have also suffered from the shortcoming. The difference is, aerosol and cloud hydrometeor particles are discretely size and composition resolved and move in 3-D in the present study relative to other models that have been run at this resolution (Table 1).

[25] Several previous high-resolution Eulerian models that have treated 3-D clouds have suffered from a problem of spurious production of cloud-edge supersaturations caused in part by truncation errors in the fine-difference approximation to advection and in part by not resolving the cloud edge, as described by *Stevens et al.* [1996]. Since water vapor, all other gases, all aerosol particles and their constituents, and all hydrometeor particles and their constituents are advected here with the monotonic, bounded, and nonoscillatory advection scheme of *Walcek and Aleksic* [1998], the advection problem described should not apply to the same extent in this study. Error will arise, though, due to the lack of resolution at cloud boundaries, but the error is outweighed by the model's coverage of an entire urban airshed.

4. Emissions and Simulation Setup

[26] Global-through-urban nested simulations were run for February and August 1999 to compare results with data and to examine the feedbacks of aerosol particles. The baseline emission inventory for the U.S. was the 1999 National Emission Inventory, version 2 [*USEPA*, 2003a]. Pollutants emitted hourly included the gases CO, CH_4, paraffins, olefins, formaldehyde, higher aldehydes, toluene, xylene, isoprene, monoterpenes, NO, NO_2, HONO, NH_3, SO_2, SO_3, and H_2SO_4 and the particle components black carbon (BC), primary organic matter (POM), sulfate, and nitrate. Additional emission types, not in the NEI, included biogenic gases (isoprene, monoterpenes, other volatile organics, and nitric oxide), wind-driven soil dust, sea spray, pollen, spores, bacteria, NO_x from lightning, ocean DMS, volcanic SO_2, many gases and particles from biomass burning, and CO_2, H_2, and H_2O from fossil-fuel combustion and biomass burning. Emissions outside the U.S. were calculated as in *Jacobson* [2006]. From the raw U.S. inventory, inventories were prepared for each model domain, including the global domain. Annual anthropogenic emissions into the SCAB domain were 4.7 MT/a (megatonnes/a) CO, 0.66 MT/a NO_x as NO_2, 0.9 MT/a ROG, 0.26 MT/a CH_4, 0.042 MT/a SO_2, 0.075 MT/a sub-2.5-μm primary organic carbon, 0.014 MT/a sub-2.5-μm BC, 0.0055 MT/a sub-2.5-μm sulfate, 0.00053 MT/a sub-2.5-μm nitrate, and 0.121 MT/a sub-2.5-μm other material, and additional coarse-mode particulate matter. Particle mass emissions were distributed over multimodal lognormal distributions then discretized into size bins.

[27] Two simulations were run for each February and August 1999: one with baseline emissions of gas and aerosol components and one in which all anthropogenic aerosol particle and precursor gas (AAPPG) emissions were removed from the SCAB domain only. Particle emissions removed included anthropogenic BC, POM, S(VI), and nitrate. Precursor gases removed included anthropogenic SO_x, NH_3, NO_x, and speciated nonmethane organic gases (which also affect photochemical smog), but not CO_2, CH_4, N_2O, or CFCs. The global and California domain simulations were the same for both the baseline and sensitivity SCAB simulations to ensure that errors due to coarser resolution in the parent California and global domains did not influence results in the finer SCAB domain. Inflow for both SCAB domain simulations originated from the California domain; inflow for the California domain originated from the global domain.

[28] The time interval for nesting was one hour. Variables passed at horizontal boundaries included temperature, specific humidity, wind velocity, gas concentrations (including total water as water vapor), and size- and composition-resolved aerosol number and mole concentrations. A five-row buffer layer at each horizontal boundary in each fine domain was used to relax concentrations and other variables [*Jacobson*, 2005d, Section 21.1.11]. Clouds did not cross domain boundaries since total water moved across boundaries in the form of water vapor and could generate new clouds; however, clouds could be passed across the boundaries for future studies.

[29] Initial 3-D meteorological fields were obtained from National Center for Environmental Prediction (NCEP) reanalysis fields for 1 February and 1 August 1999, at 12 GMT [*NCEP*, 2003]. In the U.S., surface meteorological data from over 1650 stations [*USEPA*, 2003b] were assimilated with the NCEP data for each domain. Aerosol and gas fields in all domains were similarly initialized from background data. U.S. EPA ambient air quality data [*USEPA*, 2003b] for O_3, CO, NO_2, SO_2, $PM_{2.5}$, and PM_{10} were then assimilated with background values at the initial time. No data assimilation, nudging, or model spinup was performed at any point past initialization.

5. Comparison of Baseline Results With In–Situ Data

[30] In this section, baseline model results for February and August 1999 are compared with data to evaluate model performance. Previous high-resolution quantitative evaluations of the model without detailed cloud treatment were done by *Jacobson* [1997b; 2001b]. In the latter study, comparisons of numerous parameters were compared with data at each of two stations and other parameters were compared at multiple stations. Figures 1 and 2 compare model predictions for February and August 1999 with hourly data, paired in time and space at the times and locations of the data. Only a few comparisons are shown since the purpose of the comparisons is to re-evaluate, rather than provide an original evaluation of the model. Air pressure was predicted accurately for a month (normalized gross error of 0.1%, or 1 hPa, over all hours of August) under high-pressure conditions. Because the model was not spun up, restarted, or assimilated with data, it effectively

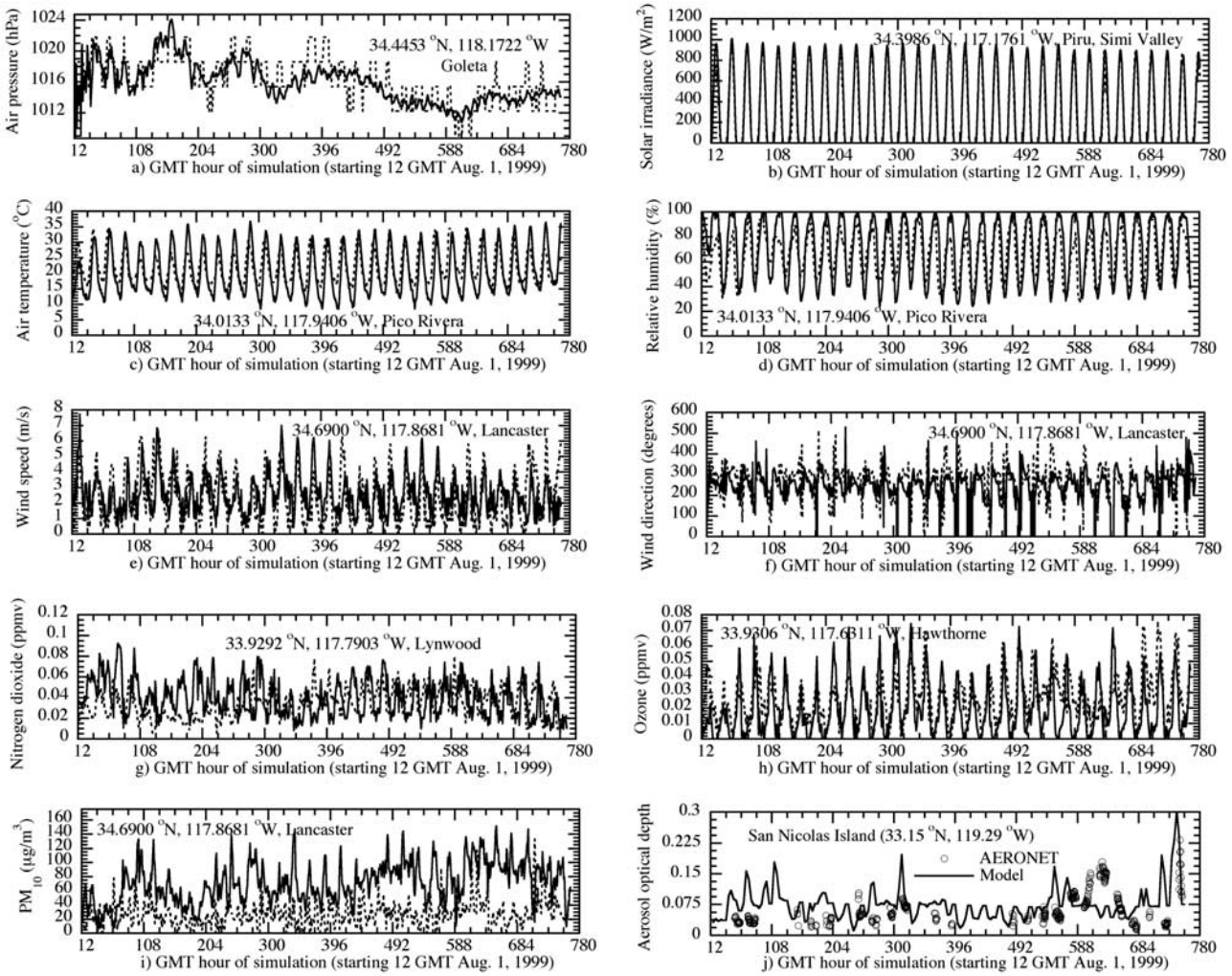

Figure 1. Comparison of August 199 hourly model predictions (solid lines) with paired-in-time-and-space data (dashed lines or open circles) for several parameters. Model results were interpolated with bilinear interpolation from four surrounding grid cell centers to the exact location of the measurement. The time resolution of data and model values was 1 hour. Data were from *USEPA* [2003b], except for (j), which were from the AERONET database [*R. Frouin, pers. comm.*].

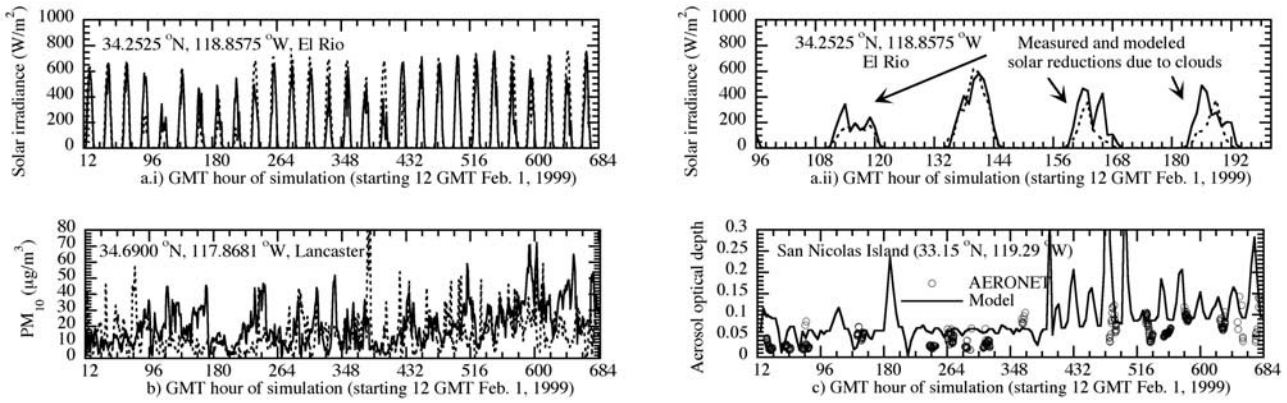

Figure 2. Same as Figure 1, except for February. The second solar irradiance panel (Figure 2.a.ii) shows a close-up of four days from the first panel to illustrate model versus measured values during a period when clouds reduced sunlight for three of the four days.

Table 2. Normalized Biases (NB) and Normalized Gross Errors (NGE) for Several Near-Surface Parameters in February and August[a]

	February			August		
	No. obs.	NB, %	NGE, %	No. obs.	NB, %	NGE, %
Temperature, K	18,695	−2.1	2.3	20,210	−0.74	1.38
Air pressure, hPa	1348	+0.46	0.62	2954	+0.051	0.28
Wind speed, m/s	12,867	+32.0	69.0	15,007	+3.77	50.7
Wind direction, deg.	11,415	+1.8	23.6	13,583	−3.3	21.5
Ozone, ppbv	784	−32.1	32.6	7165	−29.9	32.2

[a]Cutoffs were 1.5 m/s for wind speed and 50 ppbv for ozone. No other cutoffs were assumed.

predicted (after the fact) the air pressure and its trend at this location for 31 days. Table 2 shows that the normalized gross error (NGE) in air pressure over all stations and hours in the basin was 0.28% in August and 0.62% in February. Solar radiation was similarly predicted well (Figure 1b). The diurnal cycles of temperature and relative humidity were predicted consistently, but minimum or maximum temperatures were off by 5–8 K on some days (Figure 1c) and the relatively humidity was off by 30–40% on some days (Figure 1d). The model predicted the timing of the daily sea breeze quite well every day and the magnitude on many days of August (Figure 1e). Shifts in direction were also predicted although the magnitudes of the shifts were not always correct (Figure 1f).

[31] Observed titration of nighttime ozone was predicted in some locations, but not all (Figure 1h). The NGE for ozone was about 32% in August and February (Table 2). Modeled PM_{10} was generally higher than measured PM_{10} in August. Modeled aerosol optical depth at San Nicolas Island, just outside the Southwestern border of the SCAB domain, was reasonably accurate most of the month, less accurate near the end, but very accurate on the last day of the month (Figure 1j). The mean modeled August 550-nm aerosol optical depth (AOD) (0.076) was close to that observed (0.065).

[32] Figure 2 compares February modeled and measured parameters relevant to aerosols and clouds. Surface solar irradiance (Figure 2a) is relevant to clouds because low daytime values in surface solar indicate the presence of clouds. The model predicted the observed presence or absence of clouds on 25 of the 28 days in February at a specific location, with errors on the 10th, 17th, and 27th days (Figure 2.a.i). On four consecutive days (5th–8th), blown up in Figure 2a.ii, the model predicted the correct magnitude of solar reduction due to clouds. Only clouds could have reduced both modeled and measured solar radiation to the extent shown in the figure.

[33] The comparison of modeled with measured PM_{10} in February (Figure 2b) was better than in August (Figure 1i) during most of the month. The overprediction in August relative to February may be due to excessive primary coarse particle emissions (natural or anthropogenic), in both cases but lesser wet removal in August. Figure 2c compares modeled with measured aerosol optical depth at San Nicolas Island. Modeled AODs were close to measured AODs for much of the month although a few unobserved modeled spikes appeared. The spikes may have been due to surges in wind-driven sea spray.

[34] Table 3 compares modeled with measured February- and August-averaged aerosol component concentrations at a remote site in the San Bernardino Mountains. The table indicates excellent agreement for black carbon, sulfate, and sodium but less accuracy for organic carbon and nitrate. The organic carbon overpredictions are likely due to overestimates in the emission inventory. The nitrate underestimate is at relatively small nitrate concentrations for Los Angeles and could be due to chemistry, transport, or deposition errors.

6. Comparison of Baseline Results With Climatological Satellite and Other Data

[35] In order to evaluate the model further, February and August 1999 baseline result were compared with 2002–2004 climatological MODIS satellite data and with February and August 1999 precipitation data. MODIS data did not exist for 1999, but the model was run for 1999 since the emission inventory and all other data compared here were for 1999. Although the model year did not fall within the MODIS period, a qualitative comparison between 1999 and 2002–2004 is still useful since aerosols and clouds spatial distributions should not vary substantially between years. Magnitudes of aerosol and cloud properties, though, may vary more between years than spatial distributions.

[36] The AOD comparison (Figures 3a–3d) indicates relatively good correlation in space of the peak locations of modeled with climatological AOD in both months. Peak MODIS AODs, though, were slightly larger than were modeled AODs, most likely because (a) MODIS may overpredict AOD over land by about 0.07 [*Remer et al.*, 2005] and (b) MODIS AODs were determined only when clouds were absent; modeled AODs were obtained in the presence or absence of clouds. Model and emission rate uncertainties may have also affected the comparison.

[37] The cloud optical depth (COD) comparison (Figures 3e–3h) indicates lower modeled than MODIS CODs in February but not August. This result is consistent with the fact that February 1999 was drier (in terms of precipitation) than was 2002–2004. Modeled and MODIS CODs correlate well in space and magnitude over water in February and August and over portions of land in August, but not so well over land in February. The fact that MODIS values were morning averages whereas the model values were 24-h averages gave rise to some differences.

[38] Modeled cloud fractions in February and August peaked at 0.9, consistent with the MODIS retrievals, but most modeled cloud fractions over the ocean were about

Table 3. Measured Versus Modeled February- and August-Averaged Particle Concentrations at the San Gorgonio Wilderness Site in the San Bernardino Mountains (SAGO1, 34.1924N, 116.9013W, 1705 m)

	February			August		
	Data	Model	% Diff.	Data	Model	% Diff.
BC	0.26	0.3	+15	0.37	0.41	+11
OC	0.95	1.8	+89	1.6	3.9	+144
NO_3^-	2.1	0.7	−67	1.8	0.7	−61
SO_4^{2-}	0.40	0.45	+13	1.2	0.6	−50
Na^+	0.059	0.048	−19	0.10	0.09	−10

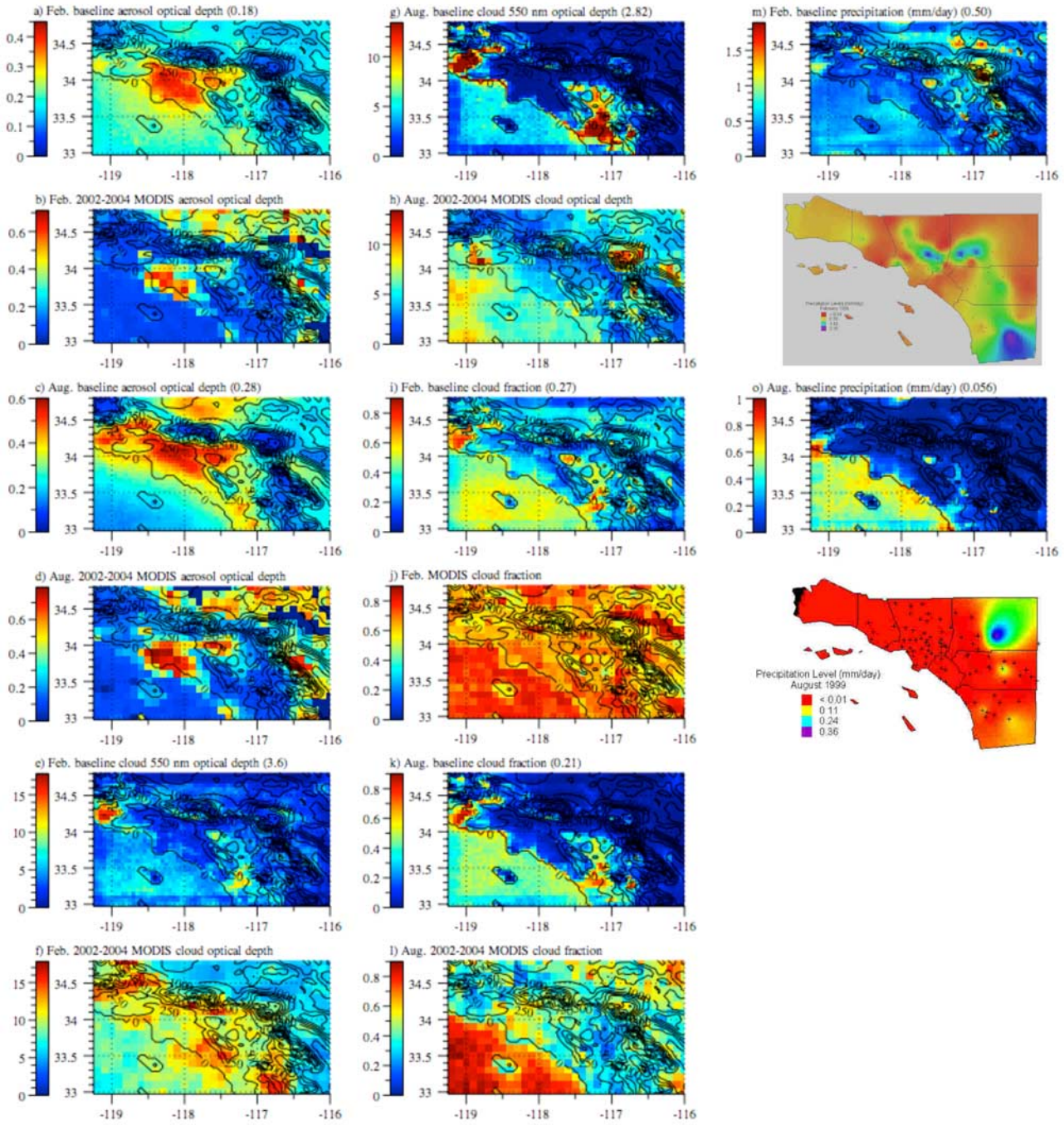

Figure 3. Comparison of February and August 1999 baseline model predictions (0800–1200 local time) with February and August 2002–2004 climatological MODIS data (1000–1100 local time) for aerosol optical depth, cloud optical depth, and cloud fraction and with February and August 1999 measured precipitation (derived from Western Regional Climate Center data by Gina Lopez and Guido Franco). Altitude contours are in meters. Numbers in parentheses are average parameter values over all land points. For Figure 3n, the legend is red: <0.03; yellow: 0.03–0.7; light blue: 0.7–1.43; purple: 1.43–2.16 mm/day.

0.6, whereas MODIS values were near 0.8 (Figures 3i–3l). Both modeled and MODIS cloud fractions, though, were remarkably lower over Catalina Island than the ocean nearby. Also, both changed value distinctly at the coastline in August, but less so in February. Differences in modeled and MODIS cloud fraction arose in part because modeled values were calculated by summing up the cross-sectional area concentrations ($cm^2\ cm^{-3}$) of all hydrometeor particles in a model grid cell, multiplying by the thickness of the cell, and summing the result among all cells in a column and limiting the result to unity. This method gives the true upper limit to the cloud fraction. MODIS cloud fractions were 1 if

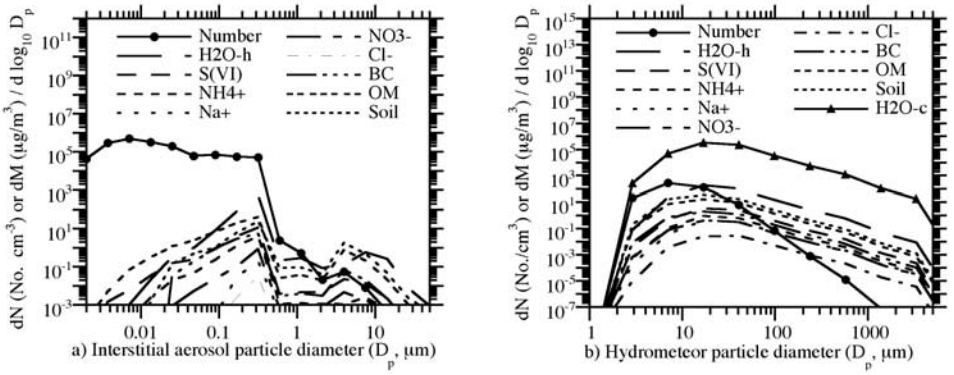

Figure 4. Modeled (a) interstitial aerosol and (b) liquid hydrometeor size distributions at 0900 Pacific Standard Time on 1 February 1999, 5 h after the start of the baseline simulation, at 33.96°N, 118.25°W (near Marina Del Rey, California), and 30 m above the topographical surface. Chemicals in the hydrometeor particles originated from aerosol particles or gases. "H2O-h" is liquid water hydrated to solute and "H2O-c" is condensed liquid water." The "Number" curve has units dN (No. cm^{-3})/ dlog$_{10}$D$_p$. All other curves have units dM (μg m^{-3})/dlog$_{10}$D$_p$.

a cloud was identified and 0 if not. Thus MODIS fractions should generally exceed model fractions. Both modeled and MODIS cloud fractions were higher under the Los Angeles aerosol plume (below the 250-m contour) than in surrounding areas, suggesting an aerosol enhancement of cloud fraction. This enhancement is demonstrated shortly.

[39] The magnitudes of modeled peak precipitation in February were relatively consistent with 1999 data (Figures 3m–3n), particularly considering 1999 had unusually low February precipitation in Southern California. Several locations of predicted and measured precipitation were also consistent [e.g., in the San Bernardino Mountain range, to the east of the Los Angeles basin, and the San Gabriel Mountains, to the north of the basin]. Differences can be seen in the Santa Ana Mountains (in the southern part of the basin). August measured and modeled precipitation were low (Figures 3o–3p). Some modeled precipitation occurred onshore and offshore near the coast due to fog deposition.

7. Analysis of Modeled Hydrometeor Size Distributions and Composition

[40] In an effort to evaluate some of the 3-D model's new cloud treatment, snapshots of modeled hydrometeor and aerosol size distributions at one altitude (Figure 4) and vertical profiles of vertical velocity and cloud water (Figure 5) are provided. In the first case, results were obtained near Marina Del Rey, California, close to the coast. In the grid cell (centered 30 m above the surface), an advection fog formed on aerosol particles. The fog extended about 200 m (three grid cells) above the surface. Aerosol particles primarily larger than 0.3-μm diameter activated. The total number concentration and liquid water content of the fog at that time were 165 drops/cm^3 and 0.25 g/m^3, respectively, and the mean number diameter was 7–15 μm, all within range of typical values [e.g., *Pruppacher and Klett*, 1997, Figures 2–4].

[41] Figure 4 shows that many new traffic-emitted interstitial nanoparticles had not yet coagulated with cloud drops and the presence of a sharp transition between activated and unactivated aerosol particles. Such a transition is not possible to obtain with a scheme where aerosols are represented by modes [e.g., *Zhang et al.*, 2002]. The individual aerosol components in the cloud drops were distributed roughly proportional to the mass size distribution of condensed liquid water. The figure demonstrates the lack of noise in the numerical schemes used. The peak concentrations in the

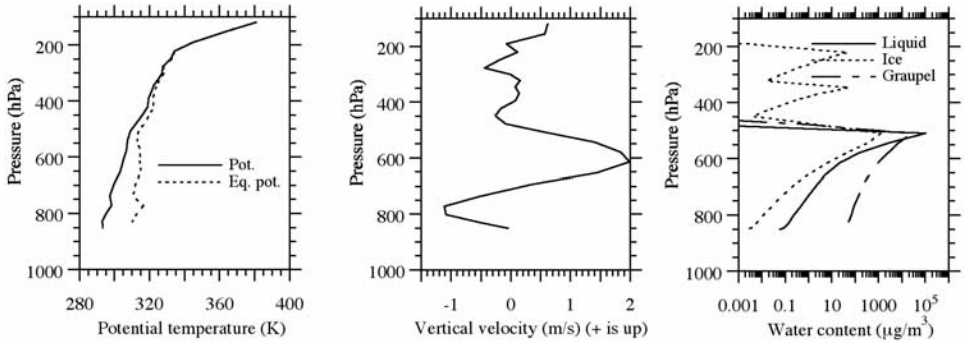

Figure 5. Vertical profiles of vertical velocity, potential temperature and equivalent potential temperature, and liquid, ice, and graupel content at 1630 Pacific Standard Time on 5 February 1999 in an altocumulus cloud to the east of the San Jacinto Mountains, California (33.3°N, 116.35°W).

figure are sharp peaks when viewed with a linear rather than logarithmic vertical axis.

[42] Figure 5 shows modeled instantaneous vertical profiles of several cloud parameters in a column to the east of the San Jacinto Mountains in the afternoon of 5 February 1999. From equivalent potential temperature, the air was slightly unstable from 650 to 500 hPa, and vertical velocities were up to 2 m/s (upward), typical for a shallow convective cloud [e.g., *Pruppacher and Klett*, 1997]. A 2-km thick mixed-phase cloud containing supercooled liquid water, ice, and graupel, formed and rose up to 500 hPa, where a clear stable layer stopped its ascent The liquid water content was up to 0.1 g/m^3. Below the main portion of the cloud, most of the water was graupel due to liquid-ice, liquid-graupel, and ice-graupel coagulation in falling hydrometeor particles. Most of falling particles also evaporated or sublimated, before reaching the ground, which was near 900 hPa. Thin low-concentration layers of ice formed above the cloud top.

8. Spatial Differences in Aerosol Parameters

[43] In this section, the modeled spatial changes in aerosol mass and optical depth due to AAPPG emissions are examined. The particle components affected most by AAPPG emissions included BC, POM, secondary organic matter (SOM), S(VI), NH_4^+, NO_3^-, and H_2O(l). Of these, BC and POM are emitted only. The others form by gas-to-particle conversion and emissions.

[44] The peak increases in BC due to AAPPG (Figure 6a) were greater in August than February, primarily because precipitation removed more BC in February than in August. Although emitted BC is relatively hydrophobic, it becomes coated by hygroscopic material and is readily removed by precipitation (through nucleation scavenging and aerosol-hydrometeor coagulation) more as it ages. Although only one internally mixed aerosol size distribution was treated, newly emitted particles near emission sources dominated many size bins, so these size bins were relatively externally mixed until particles in them aged.

[45] Modeled SOM formed from biogenic organic (e.g., isoprene and monoterpene) and anthropogenic organic (e.g., toluene and xylene) gas oxidation followed by condensation of low vapor-pressure products. The enhancement of SOM due to AAPPG (Figure 6b) was greater in August than in February due to greater oxidation of organic gases, less wet removal of SOM, and greater biogenic emissions in August than in February. Because SOM formed in the atmosphere, it spread wider than did POM, which was emitted. Near-surface particle S(VI) increased more in August than in February (Figure 6c). Although precipitation removed more sulfate in February than in August, more sulfate was produced by aqueous oxidation within aerosol particles, fog drops, and cloud drops in February than in August.

[46] The major aerosol component to decrease in concentration over land due to AAPPG was the chloride ion, whose sources were sea spray, fires, and biofuel burning. As chloride in sea spray (the dominant source) flowed over land, nitric and sulfuric acid (from emitted AAPPG species NO_x and SO_x), acidified the sea spray, expelling 16% and 52% of chloride as HCl in February and August, respectively (Table 4). Such sea spray acidification is commonly observed in coastal environments [e.g., *Hitchcock et al.*, 1980].

[47] AAPPG increased AOD over land by 20% in February and 32% in August (Table 4 and Figure 6d). This was less than the full anthropogenic contribution to AOD because the model was initialized with and treated inflow of anthropogenic and natural aerosols in both the baseline and sensitivity simulations. Thus not all initial or boundary anthropogenic material could be removed in the sensitivity (no-AAPPG) simulation during a month. For example, in February, about 89% of initial/boundary anthropogenic BC was removed, and in August, only 75% was removed (Table 4). Most of the material not removed was from initial conditions rather than inflow, since all SCAB boundaries were rural or ocean. Because only 75–89% of primary aerosols were removed in the sensitivity simulation, the results shown next are conservative and underestimate anthropogenic aerosol effects by at least this quantity.

9. Effects of Aerosols on Urban/Regional Climate Parameters

[48] Here, the effects of the changes in anthropogenic aerosol parameters from section 8 on climate parameters are discussed. AAPPG increased cloud optical depth (COD) over land by about 20% in February and 7% in August (Table 4 and Figure 6e). The larger effect in February occurred because clouds were more prevalent and the relative humidity higher in February. The increase in COD combined with the increase in aerosol particle number concentration (Table 4) due to AAPPG demonstrates the first indirect aerosol effect. Increased cloud optical depth in August occurred primarily near the coast, where the relative humidity was high and anthropogenic particles were present. Increases occurred at all altitudes but more in the boundary layer (Figure 7a) due to the greater abundance of clouds there. Because of the Pacific high, clouds in Los Angeles, particularly in the summer, are dominated by low-lying fog and stratus.

[49] AAPPG similarly increased cloud fraction (Figure 6f) and liquid water (Table 4), particularly along the coast. These results show by cause and effect what has been shown by correlation using satellite data [*Koren et al.*, 2005; *Kaufman et al.*, 2005]. AAPPG increased cloud fraction by reducing precipitation, which increased cloud liquid water and lifetime. Enhanced liquid water increased cloud drop size, and enhanced lifetime increased cloud spreading. Increased drop size and spreading increased cloud fraction up to 10 percent locally in February and August. Average column cloud liquid increases over land were 8% in February and 2% in August (Table 4). Column cloud ice increases were about 0.1% in February and 1% in August although hardly any cloud ice formed aloft in August (Table 4).

[50] AAPPG reduced net down minus up surface total solar irradiance over land (averaged over day and night) by about 2.4% in February and 1.8% in August (Figure 6g and Table 4). Reductions over water were larger (6.8% and 7.1%, respectively) because of the greater influence of AAPPG on clouds over water. AAPPG increased net down minus up thermal-IR irradiance (Table 4) in locations where aerosol and cloud optical depths increased. Peak August

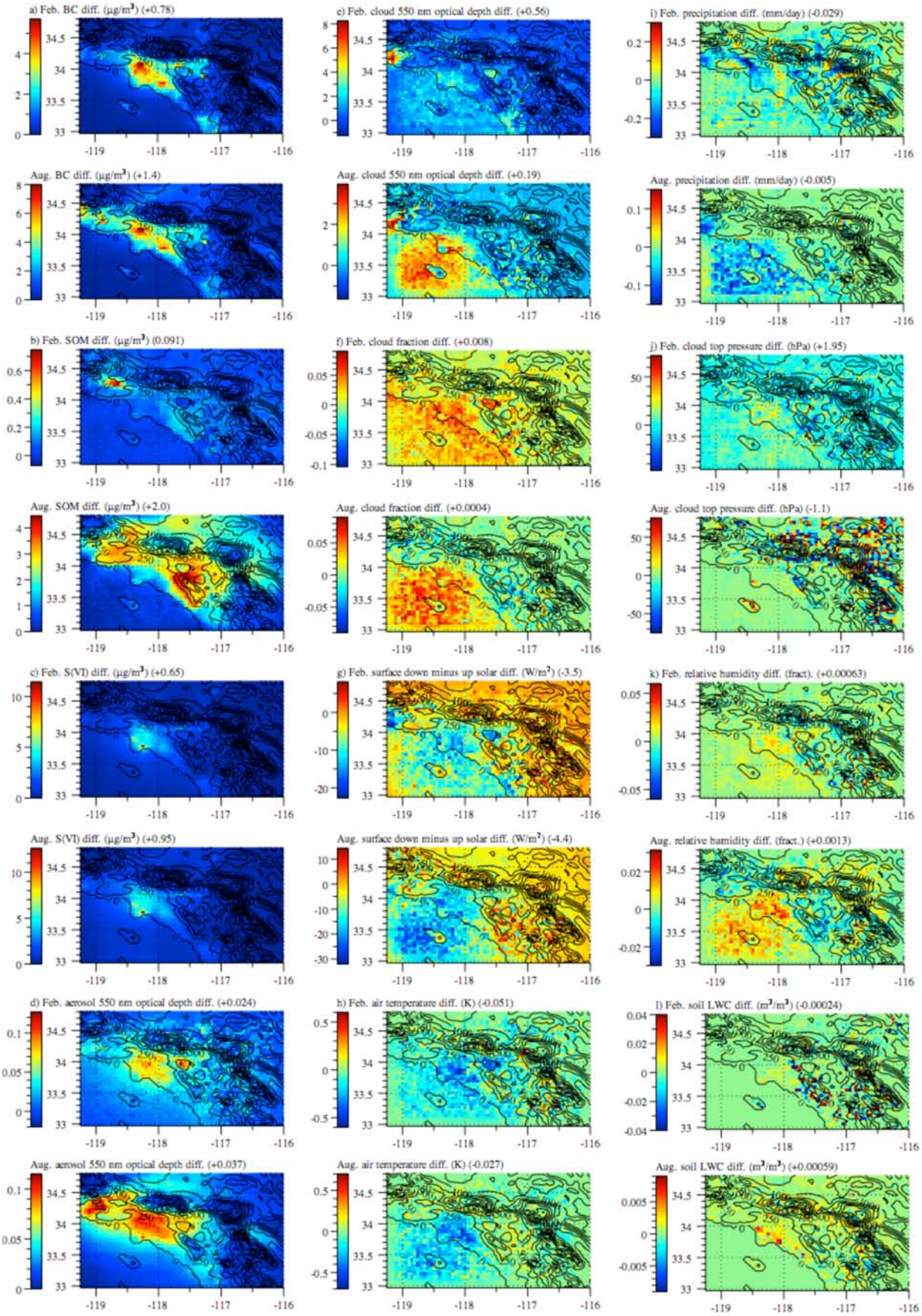
a) Feb. BC diff. (μg/m³) (+0.78)
e) Feb. cloud 550 nm optical depth diff. (+0.56)
i) Feb. precipitation diff. (mm/day) (-0.029)
Aug. BC diff. (μg/m³) (+1.4)
Aug. cloud 550 nm optical depth diff. (+0.19)
Aug. precipitation diff. (mm/day) (-0.005)
b) Feb. SOM diff. (μg/m³) (0.091)
f) Feb. cloud fraction diff. (+0.008)
j) Feb. cloud top pressure diff. (hPa) (+1.95)
Aug. SOM diff. (μg/m³) (+2.0)
Aug. cloud fraction diff. (+0.0004)
Aug. cloud top pressure diff. (hPa) (-1.1)
c) Feb. S(VI) diff. (μg/m³) (+0.65)
g) Feb. surface down minus up solar diff. (W/m²) (-3.5)
k) Feb. relative humidity diff. (fract). (+0.00063)
Aug. S(VI) diff. (μg/m³) (+0.95)
Aug. surface down minus up solar diff. (W/m²) (-4.4)
Aug. relative humidity diff. (fract.) (+0.0013)
d) Feb. aerosol 550 nm optical depth diff. (+0.024)
h) Feb. air temperature diff. (K) (-0.051)
l) Feb. soil LWC diff. (m³/m³) (-0.00024)
Aug. aerosol 550 nm optical depth diff. (+0.037)
Aug. air temperature diff. (K) (-0.027)
Aug. soil LWC diff. (m³/m³) (+0.00059)

Figure 6

Table 4. Model February- and August-Averaged, Land-Averaged Baseline Values and Differences With Minus Without AAPPG

	February Baseline	February % Change w-w/o AAPPG	August Baseline	August % Change w-w/o AAPPG
Aerosol BC, $\mu g/m^3$	0.877	+810	1.86	+300
Aerosol POM, $\mu g/m^3$	7.62	+150	15.8	+69
Aerosol SOM, $\mu g/m^3$	1.17	+8.5	6.86	+41
Aerosol LWC, $\mu g/m^3$	0.452	+117	25.8	+100
Aerosol S(VI), $\mu g/m^3$	1.19	+122	1.63	+138
Aerosol NH_3^-, $\mu g/m^3$	0.452	+117	0.714	+122
Aerosol NO_4^+, $\mu g/m^3$	0.531	+47	1.06	+85
Aerosol Cl^-, $\mu g/m^3$	0.017	−16	0.025	−52
Aerosol optical depth	0.140	+20	0.151	+32
Aerosol > 0.1 μm, No/cm^3	77,300	+113	102,000	+72
Cloud optical depth	3.26	+20	2.78	+7.2
Cloud fraction	0.292	+2.8	0.133	+0.33
Cloud LWC, kg/m^2	0.00508	+7.6	0.00549	+1.6
Cloud IWC, kg/m^2	0.0174	+0.11	0.000008	+1.1
Cloud top pressure, hPa	520	+0.38	724	−0.15
Precipitation, mm/day	0.503	−5.5	0.056	−8.5
Surface solar, W/m^2	143.5	−2.4	239	−1.8
Surface UV, W/m^2	6.86	−4.1	11.4	−5.4
Surface thermal-IR, W/m^2	−77.5	−1.2	−90.9	−0.71
Air temperature, K	276.0	−0.018	292.52	−0.0091
Relative humidity (fract.)	0.731	+0.086	0.676	+0.19
Soil moisture, m^3/m^3	0.188	−0.13	0.168	+3.5

increases offset August solar reductions by about a third. Peak February increases offset February solar reductions by about half. The net reduction in surface radiation (surface solar loss minus thermal-IR gain) was greater in August than in February. Most solar and thermal-IR irradiance changes occurred in the boundary layer (Figure 7b). Solar decreases in the boundary layer were due primarily to absorption by BC.

[51] AAPPG decreased near-surface air temperatures within the Los Angeles basin and over the ocean nearby in February and August (Figure 6h). Decreases over the ocean were due in part to the reduction in solar radiation there. Temperatures increased outside the basin, partly because BC and UV-absorbing organics warmed the mid boundary layer over the basin (Figure 7c) and winds advected the warm air outside the basin, where turbulence mixed it closer to the surface. Boundary layer temperature increases were small (~0.01 K) mostly because the warming effect due to BC was significantly offset by non-BC aerosol cooling. Boundary layer warming due to BC plus ground cooling due to reduced solar radiation caused by all anthropogenic aerosols and aerosol-enhanced clouds, stabilized the boundary layer (Figure 7c), decreasing mixing depth.

[52] AAPPG reduced precipitation in the Los Angeles basin and the mountains beyond the basin in February (Figure 6i). In August, when precipitation (mostly drizzle or fog deposits) was low, most reductions occurred offshore and in the foothills of the San Bernardino Mountains. Some precipitation increases were found on the downslope sides of the San Bernardino and San Gabriel Mountains. *Givati and Rosenfeld* [2004] correlated increases in aerosols with precipitation reduction on the upslope side of mountains and with precipitation increase on the downslope side. These relationship are shown here by cause and effect. Modeled precipitation decreases in February and August over land due to AAPPG were 5.5% and 8.5% (−0.029 and −0.005 mm/day), respectively. Peak decreases were 13% and 17% (−0.25 and −0.1 mm/day) of peak precipitation, respectively.

[53] AAPPG decreased cloud top pressures over the foothills and mountains but increased them in coastal areas under heavy pollution in February and August (Figure 6j). Changes in cloud top pressures due to AAPPG are affected by at least two processes. First, *Koren et al.* [2005] suggest that cloud top pressures over the Atlantic Ocean decrease (cloud top heights increase) in the presence of pollutant particles because reduced precipitation and enhanced water vapor invigorated the clouds, causing them to last longer and grow taller. Second, it is hypothesized here that enhanced stability over land due to heavy particle pollution can decrease convection and cloud top height. Although stability is decreased at the top of the aerosol layer (Figure 7c), the increase in stability between the surface and top of the layer has a larger impact on cloud formation. The second mechanism may have dominated here within the pollution plume of Los Angeles. The dominant mechanism, though, depends on the type of cloud and pressure system present. Here, most clouds were stratus and the Pacific high was present.

[54] AAPPG increased the near-surface relative humidity (Figure 6k), mostly by cooling air near the ground rather than by increasing water vapor. Water vapor decreased under the main aerosol plume because surface cooling

Figure 6. South-Coast-domain modeled differences between the 1999 baseline simulation (with AAPPG) and the sensitivity simulation (no AAPPG emission), averaged over all hours of February (left column) and August (right column). Altitude contours are in meters. All maps not otherwise specified are near-surface maps. Numbers in parentheses are average parameter values over all land points.

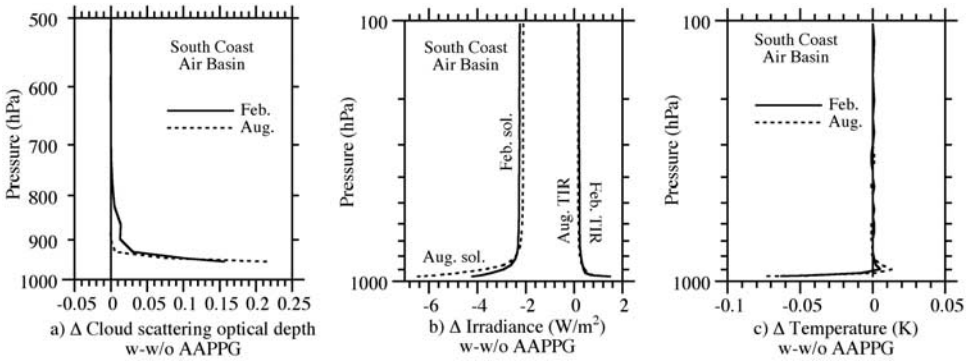

Figure 7. Modeled differences between the 1999 baseline simulation (with AAPPG) and the sensitivity simulation (no AAPPG emission) in the February and August monthly averaged, South-Coast-domain-averaged vertical profiles of some parameters. The optical depths in Figure 7a are layer, not cumulative, optical depths. The bottom temperature value in Figure 7c is ground temperature. For comparison, the monthly averaged near-surface (lowest model layer) baseline (with/AAPPG) values in February and August (respectively) for each parameter were (a) cloud scattering optical depth: 0.552, 1.12; (b) solar irradiance: 142.03 W/m^2, 233.82 W/m^2, infrared irradiance: −74.06 W/m^2, −80.75 W/m^2; (c) temperature: 276.59 K, 291.06 K.

decreased evaporation there. Some increases in near-surface water vapor occurred in mountains around the basin. The reduction in evaporation under the aerosol plume simultaneously increased soil moisture (Figure 6l), suggesting another feedback of aerosol particles to regional climate.

10. Implications for Air Quality

[55] Although the simulations were run for only two cases, each one monthlong, and isolated the effects of AAPPG in a relatively small domain (SCAB), the responses of many properties to AAPPG were consistent between months. On the basis of this consistency, it may be possible to hypothesize some additional feedbacks of AAPPG that can be examined more in future modeling and measurement studies.

[56] First, AAPPG may increase aerosol mass by increasing cloud liquid water (Table 4). Higher cloud liquid increases dissolution of soluble gases (e.g., nitric acid, ammonia, sulfur dioxide, hydrogen peroxide) into cloud drops and the rate of aqueous oxidation of sulfur dioxide to sulfate [e.g., *Kreidenweis et al.*, 2003 among others]. When cloud drops shrink, they can release their larger aerosol cores back to the air.

[57] Second, the increase in the relative humidity due to AAPPG may decrease visibility. AAPPG increased the relative humidity in both months by up to 3–5 percent (Figure 6k). An increase in the relative humidity can cause aerosol particles to swell (with greater swelling generally by inorganic than organic particles), increasing aerosol optical depth, decreasing visibility [e.g., *Poirto and Wishinski*, 1986; *Baik et al.*, 1996].

[58] Third, it is known that aerosol particles directly affect actinic fluxes and photochemistry (section 1), and that clouds affect actinic fluxes and photolysis within and below them [e.g., *Madronich*, 1987]. As such, the enhancement of cloud optical depth by aerosol particles, as found here (Figure 6e), should increase photolysis within and above the clouds and decrease photolysis below them.

[59] Fourth, by reducing precipitation, AAPPG reduced aerosol wet removal rates, increasing air pollution further. For example, the baseline black carbon concentrations in rainwater here were about 0.024 mg/L in February and 0.046 mg/L in August. The precipitation reductions due to AAPPG were 0.028 mm/day in February and 0.005 mm/day in August. Thus by reducing precipitation, AAPPG reduced the BC rainout due by 0.7 and 0.2 μg/m^2-day in February and August, respectively.

11. Conclusions

[60] The nested GATOR-GCMOM model was modified to treat the explicit 3-D evolution and movement of size- and composition-resolved clouds from size- and composition-resolved aerosol particles. The model tracks the concentrations of all aerosol inclusions and dissolved gases within size-resolved cloud and precipitation liquid, ice, and graupel over time. It also treats the interactions of interstitial aerosol particles with hydrometeor particles. The explicit treatment allows for a detailed analysis of the effects of aerosol particles on urban and regional clouds, precipitation, and climate.

[61] The model was combined with a gas and aerosol emission inventory and evaluated against in situ data and MODIS climatological data. It was then applied in global-through-urban nested mode to study feedbacks of anthropogenic aerosol particles and their precursor gases (AAPPG) to climate parameters in the South Coast Air Basin (SCAB) during February and August 1999. Because of the coarse (5 km) grid spacing and the use of a hydrostatic solution to the vertical momentum equation, errors likely occurred simulating updrafts during deep convection. Most clouds in the simulation, though, were stratus or shallow convective clouds.

[62] This study found that AAPPG increased cloud optical depth, cloud liquid water, and cloud fraction; decreased net downward surface solar radiation; increased net downward thermal-infrared radiation; decreased ground temperatures, slightly increased middle-boundary layer temperatures; increased atmospheric stability; increased the relative humidity; and decreased precipitation in the SCAB and on the upslope side of mountains beyond the basin. Stability in the basin was enhanced by a combination of warming of the air by black carbon and cooling of the ground by all particles. Enhanced stability inhibited cloud top growth under the heavy aerosol plume of the SCAB.

[63] AAPPG may feed back positively to aerosol mass by increasing cloud liquid water, thereby increasing aqueous oxidation of gases and the size of aerosol cores released upon cloud evaporation. AAPPG may also decrease visibility by enhancing the relative humidity and affect photolysis by increasing cloud optical depth. Finally, AAPPG may reduce aerosol wet removal by decreasing precipitation.

[64] **Acknowledgments.** This work was supported by the California Energy Commission's Public Interest Energy Research (PIER) program and by NASA under grants NNG04GE93G and NNG04GJ89G. We would like to thank Guido Franco and Daniel Rosenfeld for helpful comments; Gina Lopez, Guido Franco, and the Western Regional Climate Center for precipitation data; and Shana Mattoo of the NASA Goddard Space Flight Center for preparing MODIS data. We would also like to thank Robert Frouin of U.C. San Diego for establishing and maintaining the San Nicolas Island AERONET site from which data were used.

References

Abdul-Razzak, H., and S. J. Ghan (2004), Parameterization of the influence of organic surfactants on aerosol activation, *J. Geophys. Res.*, *109*, D03205, doi:10.1029/2003JD004043.

Ackerman, A. S., O. B. Toon, and P. V. Hobbs (1995), A model for particle microphysics, turbulent mixing, and radiative transfer in the stratocumulus-topped marine boundary layer and comparisons with measurements, *J. Atmos. Sci.*, *52*, 1204–1236.

Ackerman, A. S., O. B. Toon, D. E. Stevens, A. J. Heymsfield, V. Ramanathan, and E. J. Welton (2000), Reduction of tropical cloudiness by soot, *Science*, *288*, 1042–1047.

Ackerman, A. S., O. B. Toon, D. E. Stevens, and J. A. Coakley Jr. (2003), Enhancement of cloud cover and suppression of nocturnal drizzle in stratocumulus polluted by haze, *Geophys. Res. Lett.*, *30*(7), 1381, doi:10.1029/2002GL016634.

Ackerman, T. P. (1977), A model of the effect of aerosols on urban climates with particular applications to the Los Angeles basin, *J. Atmos. Sci.*, *34*, 531–546.

Albrecht, B. A. (1989), Aerosols, cloud microphysics, and fractional cloudiness, *Science*, *245*, 1227–1230.

Arakawa, A., and V. R. Lamb (1981), A potential entrophy and energy conserving scheme for the shallow water equations, *Mon. Weather Rev.*, *109*, 18–36.

Andreae, M. O., D. Rosenfeld, P. Artaxo, A. A. Costa, G. P. Frank, K. M. Longo, and M. Z. F. Silva-Dias (2004), Smoking rain clouds over the Amazon, *Science*, *303*, 133–342.

Baik, N.-J., Y. P. Kim, and K. C. Moon (1996), Visibility study in Seoul, 1993, *Atmos. Environ.*, *30*, 2319–2328.

Bergstrom, R. W., and R. Viskanta (1973a), Modeling of the effects of gaseous and particulate pollutants in the urban atmosphere. Part I: Thermal structure, *J. Appl. Meteorol.*, *12*, 901–912.

Bergstrom, R. W., and R. Viskanta (1973b), Modeling of the effects of gaseous and particulate pollutants in the urban atmosphere. Part II: Pollutant dispersion, *J. Appl. Meteorol.*, *12*, 913–918.

Borys, R. D., D. H. Lowenthal, S. A. Cohn, and W. O. J. Brown (2003), Mountaintop and radar measurements of anthropogenic aerosol effects on snow growth and snowfall rate, *Geophys. Res. Lett.*, *30*(10), 1538, doi:10.1029/2002GL016855.

Bretherton, C. S., E. Klinker, A. K. Betts, and J. Coakley (1995), Comparison of ceilometer, satellite, and synoptic measurements of boundary layer cloudiness and the ECMWF diagnostic cloud parameterization scheme during ASTEX, *J. Atmos. Sci.*, *52*, 2736–2751.

Chen, J.-P., and D. Lamb (1999), Simulation of cloud microphysical and chemical processes using a multicomponent framework. Part II: Microphysical evolution of a wintertime orographic cloud, *J. Atmos. Sci.*, *56*, 2293–2312.

Clark, T. L. (1979), Numerical simulations with a three-dimensional cloud model: Lateral boundary condition experiments and multicellular severe storm simulations, *J. Atmos. Sci.*, *36*, 2191–2215.

Danielsen, E. F., R. Bleck, and D. A. Morris (1972), Hail growth by stochastic collection in a cumulus model, *J. Atmos. Sci.*, *29*, 135–155.

Dickerson, R. R., S. Kondragunta, G. Stenchikov, K. L. Civerolo, B. G. Doddridge, and B. N. Holben (1997), The impact of aerosols on solar UV radiation and photochemical smog, *Science*, *278*, 827–830.

Ding, P., and D. A. Randall (1998), A cumulus parameterization with multiple cloud base levels, *J. Geophys. Res.*, *103*, 11,341–11,353.

Easter, R. C., S. J. Ghan, Y. Zhang, R. D. Saylor, E. G. Chapman, N. S. Laulainen, H. Abdul-Razzak, L. R. Leung, X. Bian, and R. A. Zaveri (2004), MIRAGE: Model description and evaluation of aerosols and trace gases, *J. Geophys. Res.*, *109*, D20210, doi:10.1029/2004JD004571.

Fantoukis, C., and A. Nenes (2005), Continued development of a cloud droplet formation parameterization for global climate models, *J. Geophys. Res.*, *110*, D11212, doi:10.1029/2004JD005591.

Fast, J. D., W. I. Gastafson Jr., R. C. Easter, R. A. Zaveri, J. C. Barnard, E. G. Chapman, G. A. Grell, and S. E. Peckham (2006), Evolution of ozone, particulates, and aerosol direct radiative forcing in the vicinity of Houston using a fully coupled meteorology-chemistry-aerosol model, *J. Geophys. Res.*, *111*, D21305, doi:10.1029/2005JD006721.

Feingold, G., S. M. Kreidenweis, B. Stevens, and W. R. Cotton (1996), Numerical simulations of stratocumulus processing of cloud condensation nuclei through collision-coalescence, *J. Geophys. Res.*, *101*, 21,391–21,402.

Feingold, G., and S. M. Kreidenweis (2002), Cloud processing of aerosol as modeled by a large eddy simulation with coupled microphysics and aqueous chemistry, *J. Geophys. Res.*, *107*(D23), 4687, doi:10.1029/2002JD002054.

Feingold, G., H. L. Jiang, and J. Y. Harrington (2005), On smoke suppression of clouds in Amazonia, *Geophys. Res. Lett.*, *32*, L02804, doi:10.1029/2004GL021369.

Fountoukis, C., and A. Nenes (2005), Continued development of a cloud droplet formation parameterization for global climate models, *J. Geophys. Res.*, *110*, D11212, doi:10.1029/2004JD005591.

Ghan, S. J., R. C. Easter, E. G. Chapman, H. Abdul-Razzak, Y. Zhang, L. R. Leung, N. S. Laulainen, R. D. Saylor, and R. A. Zaveri (2001), A physically-based estimate of radiative forcing by anthropogenic sulfate aerosol, *J. Geophys. Res.*, *106*(D6), 5279–5294, doi:10.1029/2000JD900503.

Givati, A., and D. Rosenfeld (2004), Quantifying precipitation suppression due to air pollution, *J. Appl. Meteorol.*, *43*, 1038–1056.

Gunn, R., and B. B. Phillips (1957), An experimental investigation of the effect of air pollution on the initiation of rain, *J. Meteorol.*, *14*, 272–280.

Hall, W. D. (1980), A detailed microphysical model within a two-dimensional dynamic framework: Model description and preliminary results, *J. Atmos. Sci.*, *37*, 2486–2507.

Hansen, J., M. Sato, and R. Ruedy (1997), Radiative forcing and climate response, *J. Geophys. Res.*, *102*, 6831–6864.

Hitchcock, D. R., L. L. Spiller, and W. E. Wilson (1980), Sulfuric acid aerosols and HCl release in coastal atmospheres: Evidence of rapid formation of sulfuric acid particulates, *Atmos. Environ.*, *14*, 165–182.

Jacobson, M. Z. (1997a), Development and application of a new air pollution modeling system. Part II: Aerosol module structure and design, *Atmos. Environ.*, *31A*, 131–144.

Jacobson, M. Z. (1997b), Development and application of a new air pollution modeling system. Part III: Aerosol-phase simulations, *Atmos. Environ.*, *31A*, 587–608.

Jacobson, M. Z. (1998), Studying the effects of aerosols on vertical photolysis rate coefficient and temperature profiles over an urban airshed, *J. Geophys. Res.*, *103*, 10,593–10,604.

Jacobson, M. Z. (2001a), GATOR-GCMM: A global through urban scale air pollution and weather forecast model. 1. Model design and treatment of subgrid soil, vegetation, roads, rooftops, water, sea ice, and snow, *J. Geophys. Res.*, *106*, 5385–5402.

Jacobson, M. Z. (2001b), GATOR-GCMM: 2. A study of day- and nighttime ozone layers aloft, ozone in national parks, and weather during the SARMAP Field Campaign, *J. Geophys. Res.*, *106*, 5403–5420.

Jacobson, M. Z. (2002a), Analysis of aerosol interactions with numerical techniques for solving coagulation, nucleation, condensation, dissolution, and reversible chemistry among multiple size distributions, *J. Geophys. Res.*, *107*(D19), 4366, doi:10.1029/2001JD002044.

Jacobson, M. Z. (2002b), Control of fossil-fuel particulate black carbon and organic matter, possibly the most effective method of slowing global

warming, *J. Geophys. Res.*, *107*(D19), 4410, doi:10.1029/2001JD001376.
Jacobson, M. Z. (2003), Development of mixed-phase clouds from multiple aerosol size distributions and the effect of the clouds on aerosol removal, *J. Geophys. Res.*, *108*(D8), 4245, doi:10.1029/2002JD002691.
Jacobson, M. Z. (2004), The climate response of fossil-fuel and biofuel soot, accounting for soot's feedback to snow and sea ice albedo and emissivity, *J. Geophys. Res.*, *109*, D21201, doi:10.1029/2004JD004945.
Jacobson, M. Z. (2005a), A solution to the problem of nonequilibrium acid/base gas-particle transfer at long time step, *Aerosol Sci. Technol*, *39*, 92–103.
Jacobson, M. Z. (2005b), A refined method of parameterizing absorption coefficients among multiple gases simultaneously from line-by-line data, *J. Atmos. Sci.*, *62*, 506–517.
Jacobson, M. Z. (2005c), Studying ocean acidification with conservative, stable numerical schemes for nonequilibrium air-ocean exchange and ocean equilibrium chemistry, *J. Geophys. Res.*, *110*, D07302, doi:10.1029/2004JD005220.
Jacobson, M. Z. (2005d), *Fundamentals of Atmospheric Modeling, Second Edition*, Cambridge Univ. Press, New York, 813 pp.
Jacobson, M. Z. (2006), Effects of absorption by soot inclusions within clouds and precipitation on global climate, *J. Phys. Chem.*, *110*, 6860–6873.
Jacobson, M. Z., and Y. J. Kaufman (2006), Wind reduction by aerosol particles, *Geophys. Res. Lett.*, *33*, L24814, doi:10.1029/2006GL027838.
Jiang, H., G. Feingold, and W. R. Cotton (2002), Simulations of aerosol-cloud-dynamical feedbacks resulting from entrainment of aerosol into the marine boundary layer during the Atlantic Stratocumulus Transition Experiment, *J. Geophys. Res.*, *107*(D24), 4813, doi:10.1029/2001JD001502.
Kaufman, Y. J., I. Koren, L. A. Remer, D. Rosenfeld, and Y. Rudich (2005), Smoke, dust, and pollution aerosol clouding the Atlantic atmosphere, *Proc. Natl. Acad. Sci.*, *102*, 11207–11212.
G. S. Ketefian (2006), Development and testing of a 2-D potential-enstrophy-conserving numerical ocean model and a 3-D potential-enstrophy-conserving nonhydrostatic compressible numerical atmospheric model. Ph.D. dissertation, Stanford Univ., ~1300 pp. www.stanford.edu/group/efmh/gsk/.
Khain, A., A. Pokrovsky, M. Pinsky, A. Seifert, and V. Phillips (2004), Effects of atmospheric aerosols on deep convective clouds as seen from simulations using a spectral microphysics mixed-phase cumulus cloud model Part 1: Model description, *J. Atmos. Sci.*, *61*, 2963–2982.
Kittelson, D. B. (1998), Engine and nanoparticles: A review, *J. Aer. Sci.*, *6*, 443–451.
Klein, S. A. (1997), Synoptic variability of low-cloud properties and meteorological parameters in the subtropical trade wind boundary layer, *J. Clim.*, *10*, 2018–2039.
Klemp, J. B., and R. B. Wilhelmson (1978), The simulation of three-dimensional convective storm dynamics, *J. Atmos. Sci.*, *35*, 1070–1096.
Kogan, Y. L. (1991), The simulation of a convective cloud in a 3-D model with explicit microphysics. Part I: Model description and sensitivity experiments, *J. Atmos. Sci.*, *48*, 1160–1189.
Koren, I., Y. J. Kaufman, L. A. Remer, and J. V. Martins (2004), Measurements of the effect of Amazon smoke on inhibition of cloud formation, *Science*, *303*, 342–345.
Koren, I., Y. J. Kaufman, D. Rosenfeld, L. A. Remer, and Y. Rudich (2005), Aerosol invigoration and restructuring of Atlantic convective clouds, *Geophys. Res. Lett.*, *32*, L14828, doi:10.1029/2005GL023187.
Kreidenweis, S. M., C. Walcek, G. Feingold, W. Gong, M. Z. Jacobson, C.-H. Kim, X. Liu, J. E. Penner, A. Nenes, and J. H. Seinfeld (2003), Modification of aerosol mass and size distribution due to aqueous-phase SO_2 oxidation in clouds: Comparisons of several models, *J. Geophys. Res.*, *108*(D7), 4213, doi:10.1029/2002JD002697.
Lee, I. Y., and H. M. Park (1994), Comparison of microphysics parameterizations in a three-dimensional dynamic cloud model, *Atmos. Environ.*, *28*, 1615–1625.
Lohmann, U., J. Feichter, J. Penner, and R. Leaitch (2000), Indirect effect of sulfate and carbonaceous aerosols: A mechanistic treatment, *J. Geophys. Res.*, *105*, 12,193–12,206.
Lu, R., and R. P. Turco (1995), Air pollutant transport in a coastal environment, II, Three-dimensional simulations over Los Angeles basin, *Atmos. Environ.*, *29*, 1499–1518.
Lynn, B., A. Khain, J. Dudhi, D. Rosenfeld, A. Pokrovsky, and A. Seifert (2005), Spectra (bin) microphysics coupled with a mesoscale model (MM5). Part 1. Model description and first results, *Mon. Weather Rev.*, *133*, 44–58.
Madronich, S. (1987), Photodissociation in the atmosphere 1. Actinic flux and the effects of ground reflection and clouds, *J. Geophys. Res.*, *92*, 9740–9752.
Mellor, G. L., and T. Yamada (1982), Development of a turbulence closure model for geophysical fluid problems, *Revs. Geophys. Space Phys.*, *20*, 851–875.
Molders, N., and M. A. Olson (2004), Impact of urban effects on precipitation in high latitudes, *J. Hydrometeorol.*, *5*, 409–429.
Napari, I., M. Noppel, H. Vehkamaki, and M. Kulmala (2002), Parameterization of ternary nucleation rates for H_2SO_4-NH_3-H2O vapors, *J. Geophys. Res.*, *107*(D19), 4381, doi:10.1029/2002JD002132.
National Centers for Environmental Prediction (NCEP) (2003), 2.5 degree global final analyses, distributed by the Data Support Section, National Center for Atmospheric Research.
Nenes, A., and J. H. Seinfeld (2003), Parameterization of cloud droplet formation in global climate models, *J. Geophys. Res.*, *108*(D14), 4415, doi:10.1029/2002JD002911.
Ovtchinnikov, M., and Y. L. Kogan (2000), An investigation of ice production mechanisms in small cumuliform clouds, using a 3D model with explicit microphysics. Part I: Model description, *J. Atmos. Sci.*, *57*, 2989–3003.
Phillips, V. T. J., L. J. Donner, and S. T. Garner (2007), Nucleation processes in deep convection simulated by a cloud-system-resolving model with double-moment bulk microphysics, *J. Atmos. Sci.*, *64*, 738–761.
Poirto, P. L., and P. R. Wishinski (1986), Visibility, sulfate and air mass history associated with the summertime aerosol in northern Vermont, *Atmos. Environ.*, *20*, 1457–1469.
Proctor, F. H. (1989), Numerical simulations of an isolated microburst. Part II: Sensitivity experiments, *J. Atmos. Sci.*, *46*, 2143–2165.
Pruppacher, H. R. and J. D. Klett (1997), *Microphysics of Clouds and Precipitation*, Kluwer Academic Publishers, Dordrecht.
Reisin, T., Z. Levin, and S. Tzivion (1996), Rain production in convective clouds as simulated in an axisymmetric model with detailed microphysics. Part I: Description of the model, *J. Atmos. Sci.*, *53*, 497–519.
Remer, L. A., Y. J. Kaufman, D. Tanré, S. Mattoo, D. A. Chu, J. V. Martins, R.-R. Li, C. Ichoku, R. C. Levy, R. G. Kleidman, T. F. Eck, E. Vermote, and B. N. Holben (2005), The MODIS aerosol algorithm, products and validation, *J. Atmos. Sci.*, *62*(4), 947–973.
Rosenfeld, D. (2000), Suppression of rain and snow by urban and industrial air pollution, *Science*, *287*, 1793–1796.
Segal, Y., A. Khain, M. Pinsky, and A. Sterkin (2004), Effects of atmospheric aerosol on precipitation in cumulus clouds as seen from 2000-bin cloud parcel microphysical model: Sensitivity study with cloud seeding applications, *Q. J. R. Meteorol. Soc.*, *130*, 561–582.
Skamarock, W. C., M. L. Weisman, and J. B. Klemp (1994), Three-dimensional evolution of simulated long-lived squall lines, *J. Atmos. Sci.*, *51*, 2563–2584.
Skamarock, W. C., J. B. Klemp, J. Dudhia, D. O. Gill, D. M. Barker, W. Wang, J. G. Powers (2005), A description of the Advanced Research WRF, Version 2, NCAR/TN-468+STR.
Stevens, B., R. L. Walko, W. R. Cotton, and G. Feingold (1996), The spurious Production of cloud-edge supersaturations by Eulerian models, *Mon. Weather Rev.*, *124*, 1034–1041.
Storelvmo, T., J. E. Kristjansson, S. J. Ghan, A. Kirkevag, O. Seland, and T. Iversen (2006), Predicting cloud droplet number concentration in Community Atmosphere Model (CAM)-Oslo, *J. Geophys. Res.*, *111*, D24208, doi:10.1029/2005JD006300.
Takemura, T., T. Nozawa, S. Emori, T. Y. Nakajima, and T. Nakajima (2005), Simulation of climate response to aerosol direct and indirect effects with aerosol transport-radiation model, *J. Geophys. Res.*, *110*, D02202, doi:10.1029/2004JD005029.
Toon, O. B., C. P. McKay, T. P. Ackerman, and K. Santhanam (1989), Rapid calculation of radiative heating rates and photodissociation rates in inhomogeneous multiple scattering atmospheres, *J. Geophys. Res.*, *94*, 16,287–16,301.
Twomey, S. A. (1977), The effect of cloud scattering on the absorption of solar radiation by atmospheric dust, *J. Atmos. Sci.*, *29*, 1156–1159.
Tzivion, S., T. Reisin, and Z. Levin (1994), Numerical simulation of hygroscopic seeding in a convective cloud, *J. Appl. Meteorol.*, *33*, 252–267.
United States Environmental Protection Agency (USEPA) (2003a), Clearinghouse for Inventories and Emission Factors, http://www.epa.gov/ttn/chief/.
United States Environmental Protection Agency (USEPA) (2003b), AIR Data, http://www.epa.gov/air/data/.
Venkatram, A., and R. Viskanta (1977), Effects of aerosol-induced heating on the convective boundary layer, *J. Atmos. Sci.*, *34*, 1918–1933.
Walcek, C. J., and N. M. Aleksic (1998), A simple but accurate mass conservative, peak-preserving, mixing ratio bounded advection algorithm with Fortran code, *Atmos. Environ.*, *32*, 3863–3880.
Walko, R. L., W. R. Cotton, M. P. Meyers, and J. Y. Harrington (1995), New RAMS cloud microphysics parameterization Part I: The single-moment scheme, *Atmos. Res.*, *38*, 29–62.

Wang, C., and J. S. Chang (1993), A three-dimensional numerical model of cloud dynamics, microphysics, and chemistry. 1. Concepts and formulation, *J. Geophys. Res.*, *98*, 14,827–14,844.

Warner, J. (1968), A reduction in rainfall associated with smoke from sugarcane fires—An inadvertent weather modification?, *J. Appl. Meteorol.*, *7*, 247–251.

Zhang, Y., C. Seigneur, J. H. Seinfeld, M. Z. Jacobson, and F. S. Binkowski (1999), Simulation of aerosol dynamics: A comparative review of algorithms used in air quality models, *Aerosol Sci. Technol.*, *31*, 487–514.

Zhang, Y., R. C. Easter, S. J. Ghan, and H. Abdul-Razzak (2002), Impact of aerosol size representation on modeling aerosol-cloud interactions, *J. Geophys. Res.*, *107*(D21), 4558, doi:10.1029/2001JD001549.

M. Z. Jacobson, Department of Civil and Environmental Engineering, Stanford University, Stanford, California 94305-4020, USA. (jacobson@stanford.edu)

Y. Rudich, Department of Environmental Sciences, Weizmann Institute of Science, Rehovot 76100, Israel. (yinon@wisemail.weizmann.ac.il)